Title
Using Biomaterials to Elicit an Immune Response and Trigger Tissue Regeneration

Author
Parks, Abigail Corrin

Publication Date
2014

Peer reviewed|Thesis/dissertation

UNIVERSITY OF CALIFORNIA

Los Angeles

Using Biomaterials to Elicit an Immune Response and Trigger Tissue Regeneration

A dissertation submitted in partial satisfaction

for the degree Doctor of Philosophy in

Biomedical Engineering

by

Abigail Corrin Parks

2014

ABSTRACT OF THE DISSERTATION

Using Biomaterials to Elicit an Immune Response

and Trigger Tissue Regeneration

by

Abigail Corrin Parks

Doctor of Philosophy in Biomedical Engineering

University of California, Los Angeles, 2014

Professor Benjamin Wu, Chair

Soft tissue loss can be the result of many clinical issues. An engineered injectable material to stimulate soft tissue regeneration would be an improvement for many clinical applications within tissue augmentation including dermal augmentation, periurethral bulking, and gingival augmentation.

Implanted biomaterials are usually held to a standard of biocompatibility meaning that the overall goal for a biomaterial is to have it as inert as possible and to act stealthily when it comes in contact with the body. This is to avoid a chronic foreign body response and ultimately rejection of the biomaterial. The goal of this project was to utilize a mild, transient immune response within the soft tissue of the body to accelerate regeneration of the extracellular matrix proteins and therefore tissue augmentation.

An injectable biomaterial was utilized to increase the volume of the soft tissue, then it was combined with a bioactive coating that elicited an immune response. The injectable material was fabricated out of macroporous poly ε-caprolactone (PCL) microparticles and

coated in the bioactive polymer, poly lactic co-glycolic acid (PLGA). The host-material interaction of the bioactive PLGA with biological cells was characterized *in vitro* by inflammatory cytokine production using a multiplex system. It was found that the co-culture of human fibroblasts and monocytes produced elevated levels of IL-1β, IL-6, GM-CSF, and TNF-α in response to the PLGA biomaterial. Subsequently, the cell infiltration, inflammatory response, blood vessel infiltration, and collagen deposition were analyzed to determine tissue regeneration and healing *in vivo.* The murine model showed more thorough tissue integration and healing with added porosity and bioactive PLGA coating through blood vessel infiltration and extracellular matrix deposition. The accelerated healing response seen with the bioactive coating is shown to be important to prevent migration of the particles within tissue. Additionally the PLGA coating did enhance the immune response early on in the *in vivo* studies corroborating with the *in vitro* findings.

The overall goal of this research was to engineer an injectable material that can be used to induce an acute immune response which will lead to the accelerated production of extracellular matrix proteins to augment tissue and eventually create a soft tissue network with the ultimate clinical application being dermal augmentation, periurethral bulking, or gingival augmentation.

COMMITTEE MEMBERS

Tara Aghaloo

James Dunn

Min Lee

Benjamin Wu, Committee Chair

2014

DEDICATION

This dissertation is dedicated to my loving husband Brian. Through this journey, he has loved and supported me. Brian, I love you more every day, so much that I didn't even know it was possible. You are MW, ME. As this chapter of my life closes, a new one opens with the birth of our first child and together we embark on many more chapters in life!

I would also like to thank my parents for their never ending support in all of my life's endeavors. Since I was a young child they have been at every event to support me and although I am no longer a child, they continue to love and support me in everything I do, including this long journey of earning a PhD. I know they will always be my biggest fans. Thank you Mom and Dad!

TABLE OF CONTENTS

LIST OF FIGURES

LIST OF TABLES

LIST OF ACRONYMS

2D	Two dimensional
3D	Three dimensional
$CaCl_2$	Calcium Chloride
CDC	Center for Disease Control
DCM	Dichloromethane
ECM	Extracellular matrix
FBS	Fetal Bovine Serum
FDA	Food and Drug Administration
GERD	Gastroesophageal Reflux Disease
GM-CSF	Granulocyte Macrophage Colony-Stimulating Factor
H&E	Hematoxylin and Eosin
IL-1β	Interleukin – 1beta
IL-6	Interleukin - 6
IL-8	Interleukin - 8
ISO	International Organization for Standardization
LPS	Lipopolysaccharide
NH_4HCO_3	Ammonium Bicarbonate
PCL	Poly ε-caprolactone
PLA	Poly lactic acid
PLGA	Poly lactic-co-glycolic acid
PMMA	Poly methyl-methacrylate
PVA	Polyvinyl alcohol
SEM	Scanning Electron Microscopy
SEM-EDS	Spectral Elemental Analysis of Scanning Electron Microscopy
SUI	Stress Urinary Incontinence

TNF-α	Tumor Necrosis Factor - alpha
VEG-F	Vascular Endothelial Growth Factor

ACKNOWLEDGEMENTS

Chase Linsley, for his dedication in reviewing and editing all of my written manuscripts.

Christopher Walthers, for his assistance with the murine animal studies included in Chapter 2 and 4 of this work and the rat gingival model in Chapter 5.

Leah Nakamura, for her surgical expertise and experimentation for the rat periurethral and subcutaneous models included in Chapter 5.

Chapter 2.1 is included with copyright permission from: © 2012 IEEE. Reprinted, with permission, from Corrin AA, Ngai M, Walthers CM, Dunn JCY, Wu BM, Injectable macroporous microparticles for soft tissue augmentation, 2012 Annual International Conference of the IEEE Engineering in Medicine and Biology Society (EMBC), 2012.

Chapter 3 is a version of a submitted work: Parks AC, Sung K, Wu BM. A Three-Dimensional *In Vitro* Model to Quantify Inflammatory Response to Biomaterials.

VITA/BIOGRAPHICAL SKETCH

Education

California Lutheran University

College of Arts and Sciences

Department of Bioengineering

Bachelors of Science, Bioengineering, Magna Cum Laude

Minor: Philosophy

University of California, Los Angeles

Henry Samueli School of Engineering and Applied Sciences

Biomedical Engineering Interdepartmental Program

Masters of Science

Teaching Experience

Teaching Associate

Henry Samueli School of Engineering and Applied Sciences

University of California, Los Angeles

Teaching Assistant

Henry Samueli School of Engineering and Applied Sciences

University of California, Los Angeles

Publications

J. J. Mack, **A. A. Corrin**, S. L. Dos Santos E Lucato, J. C. Y. Dunn, B. W. Wu, and B. N. Cox, "Enhanced cell viability via strain stimulus and fluid flow in magnetically actuated scaffolds," Biotechnol. Bioeng., Oct. 2012.

A. A. Corrin, M. Ngai, C. M. Walthers, J. C. Y. Dunn, and B. M. Wu, "Injectable macroporous microparticles for soft tissue augmentation," Conf Proc IEEE Eng Med Biol Soc. 2012, pp. 2428–2431.

J. J. Mack, B. N. Cox, O. Sudre, **A. A. Corrin**, S. L. dos Santos e Lucato, C. Ma, and J. S. Andrew, "Achieving nutrient pumping and strain stimulus by magnetic actuation of tubular scaffolds," Smart Materials and Structures, vol. 18, no. 10, p. 104025, Oct. 2009.

J. J. Mack, **A. A. Corrin**, S. L. dos S. e Lucato, B. N. Cox, J. S. Andrew, D. R. Clarke, M. Lam, J. C. Y. Dunn, and B. W. Wu, "Magnetically Actuable Scaffolds for Tissue Regeneration," ASME Conference Proceedings, vol. 2008, no. 43321, pp. 607–610, 2008.

R. G. Mooney, C. A. Costales, E. G. Freeman, J. M. Curtin, **A. A. Corrin**, J. T. Lee, S. Reynolds, B. Tawil, and M. C. Shaw, "Indentation Micromechanics of Three-Dimensional Fibrin/Collagen Biomaterial Scaffolds," Journal of Materials Research, vol. 21, no. 08, pp. 2023–2034, 2006.

CHAPTER ONE

INTRODUCTION

1.1 Background

1.1.1 Biomaterials

A biomaterial is a natural or synthetic product with an application in the medical field. Materials classified as biomaterials come into direct contact with the human body, therefore the properties of these materials are very important. The geometry, stiffness, composition, and by-products are a few of the concerns when it comes to investigating materials. Biomaterials must be FDA approved before they can be incorporated into a device or implanted into the body. FDA approval for a material consists of various levels of testing and characterizing the material for composition and material properties known as the ISO 10993. Biomaterial scaffolds are made of metals, ceramics, polymers, or composites. The material has a less likely chance of rejection if there is matching material properties between the implant and the area of the body being replaced. For instance, in bone research and regeneration, metals or ceramics are used because their stiffness closely mimics the natural tissue(1). However, these same materials should not be used for nerve regeneration because nerves are very soft and sensitive. The current research project focuses on soft polymers because the tissue of interest is soft, connective tissue within the body. The reason for strategically matching the properties is in an effort to obtain tissue in-growth and subsequent anchoring of the material to the existing tissue to augment the area.

Biomaterials have been studied and the ultimate goal during fabrication and testing is to achieve the most inert, biocompatible material possible (2). The biocompatibility of a material which is to be implanted is tested *in vitro* for cell attachment, proliferation and differentiation. If a material is cytotoxic it is considered to be non-biocompatible (3). When tested *in vivo*, the

desirable effect of a material is a non-effect; meaning that a material should not have a significant immune response and if it does, it is considered non-biocompatible.

1.1.2 Inflammation – scar formation

Inflammation around an implant is the standard reaction from the body when a foreign body is introduced. The inflammatory response is orchestrated by many different cell types releasing a variety of signals to the surrounding tissue. An implant can be phagocytosed or exfoliated from the body if there is a significant, long-lasting immune response. As part of the healing process, an acute inflammatory response occurs followed by granulation tissue formation and healing. This healing can result in fibrous encapsulation of the implanted material which can wall off the material from interaction with the body. This scar formation can be very undesirable in many applications (4–6). Specifically, with dermal injectables, an immune response is undesirable because it can cause redness, irritation, and uneven fibrous masses which are aesthetically unappealing (4,5). There are many researched methods to reduce scar formation from surgical procedures or trauma (4,9–12).

The aim of this research is to alter the view that inflammation and scar formation is undesireable. With the right tools and understanding, a transient, acute inflammatory response can initiate the deposition of tissue within the body and utilize scar formation in the process of soft tissue regeneration. A chronic inflammatory response is not desired, therefore the material which induces inflammation must exist for a period of time which is sufficient to stimulate growth in the tissue, but short-lived enough to dissipate before the long term response sets in. One current application for a biomaterial which stimulates an immune response leading to extracellular matrix production is in vascular aneurysms.

1.1.3 Aneurysm Evidence

A vascular cerebral aneurysm is the weakening of the vessel wall which leads to a protrusion from the vasculature. The danger with aneurysms is their potential to burst and

cause leakage into surrounding brain tissue. This can lead to paralysis or other devastating results. The two most typical treatments for aneurysms are endovascular coiling and craniotomies with surgical clipping. A report shows higher independent survival rates with endovascular coiling (13). Endovascular coiling is less invasive and relies on the inherent foreign body reaction to induced healing around the coils and therefore occlude the aneurysm. Endovascular bare platinum coils have been improved upon by introducing coatings, or additional materials to the surface to increase the reaction to the coil and decrease healing times (14,15).

It has been shown with clinical aneurysm data that poly lactic-*co*-glycolic acid (PLGA) can induce a shorter healing time and more extracellular matrix production around metal coils (14,15). Quick healing times are important in the application because of the sensitivity to clot formation and dislodgement of a clot with risk of subsequent emboli. When PLGA is added to the aneurysm coils, faster matrix deposition and healing is observed. This healing can be varied by the type and combination of the bioabsorbable polymeric material. The increase in scar formation leads to occlusion of the open aneurysm and a reestablishment of the continuity in vasculature.

The positive response to scar formation is unique in this vascular model, however, this project attempts to take the vascular model of healing in aneurysms and extend it to apply to soft tissue regeneration.

1.1.4 Dental Application

According to the CDC, Dental care is about $60 billion per year. Periodontitis occurs in about 86% of adults over the age of seventy. Periodontitis is the chronic inflammation of the tissues surrounding the teeth. Bacteria create colonies and begin destruction of the supporting tissues (16). Periodontitis can cause, or contribute to, the occurrence of many other dental problems such as papilla or gingival recession.

The inter-dental papilla is the gum tissue between the teeth. The main functions of the inter-dental papillae are to serve aesthetic purposes and to form a biological barrier to microbial invasion. In similar fashion to most gingival tissues, this triangular section of tissue is unable to regenerate. Papilla or gingival recession can occur due to multiple factors which include, but are not limited to: periodontal disease, surgical excision, tooth extraction, gingival biotype and root divergence (17). Excessive brushing or orthodontics which move teeth too quickly, or move them out of the alveolar plate can also lead to gingival recession (18). Some factors influencing the presence of papillae are the root proximity, bone support and gingival biotype. A distance of less than 5mm from the inter-dental contact point to the crest of the alveolar bone is more likely to sustain a papillary structure. The underlying osseous support is a large deciding factor in the presence of the papilla, without proper bone contact, the papilla is more likely to recess. The maximum distance to sustain the papilla decreases for adjoining dental implants. It is more difficult to keep the papilla intact between two dental implants. Thick gingival tissue is characteristic of fibrous tissue that resists recession, whereas thin gingival biotype has less osseous support and a lower blood supply, therefore predisposing thin gingiva to recession (17). This could suggest that a decrease in vascularization leads to gingival recession and that a sustained level (or an increase) in vascularization retains the gingival tissue in proper proportions.

The rate of occurrence of gingival recession (1mm or greater) was found to be 58% of the population of persons 30 years and older (19). Gingival recession is more prevalent in the older community; the population of 55 and older has a gingival recession rate of 83.7% (16). As the overall population ages, gingival/papillae recession will become a more prominent issue.

Papilla reconstruction is very challenging due to the small dimensions of the area in question and the unpredictability of the outcome. Swelling after procedures and lack of blood supply can further skew the expected outcomes. To restore the papilla, or other gingival tissue,

there are a few microsurgical techniques. One such technique is the use of an autologous graft to augment the area and then hold it in place with a suspension suture. This technique may help facilitate the retention of papillary height as well as apical gingival height, as compared to no surgical intervention (20,21). Other surgical techniques include various types of incisions or suture placements as well as augmenting underlying connective tissue or bone to regain the papillary region (20). However, there are limitations to these methods in that the source of grafting material is limited and the results are not sure to completely occlude the space left by the absent papilla. A majority of the microsurgical techniques are based on the survivability of donor tissue as well as the specific size of augmented material and these parameters are very hard to predict. Therefore, autologous grafts have many potential problems including the donor site morbidity, lack of supply and overall retention of the graft (22).

To address the issue of creating an extra wound via the donor site, there are microsurgical techniques being performed using acellular dermal matrix allografts to augment the area (23). One such graft is made by Alloderm. The material is human dermal skin which has had all cells (and potentially antigenic material) removed leaving an intact collagen and elastin matrix behind (24). This matrix is rehydrated, trimmed to size, then implanted using a similar microsurgical technique to that of an autograft surgery. With all the microsurgical techniques healing times are on the order of months post-surgery. This long healing time is not conducive to the original goal which was to improve aesthetics of the oral cavity.

There is a need for a less invasive technique to sustain and augment gingival tissue. The goal is controlled tissue regeneration through a mild-transient immune response and subsequent extracellular matrix protein secretion and fibrous encapsulation of the injected material.

1.1.5 Periurethral Application

Urinary incontinence affects many people and this disorder can have devastating social consequences due to the loss of urine occurring during normal, daily activities. Stress urinary incontinence (SUI) is a loss of urine due to abdominal pressure, including: coughing, sneezing, or walking. In 2006, urinary incontinence was determined to be in over 200 million people in the world (25). Additionally, the direct costs in the US were $16.3 billion for treatment, of which a majority was for women with the disorder. SUI is a lack of urethral resistance to overcoming bladder pressure (26).

Treatment for SUI depends on the rate of occurrence and the severity of the disorder. Absorptive devices and pelvic floor muscle exercises may be enough for some women to cope with incontinence, however there are also medications and devices to help for moderate cases. For long lasting and extreme SUI, surgery may be required, of which there are many types including bulking agents, tapes and slings, and colposuspensions (26,27). Surgical intervention can be daunting to the patient because of the pre-conceived notion that there can be long hospital stays and permanent need for self-catheterization. This, along with the social taboo associated with incontinence makes many women afraid to consult with their physicians on the condition (25–27).

Less invasive procedures such as bulking agents or microsurgical tapes may be better suited for most SUI patients due to the shorter recovery times and better quality of life. Bulking agents offer promise and have been used for decades in sphincter bulking (28), however there are currently very few FDA approved periurethral bulking agents and they require re-injection quite often (28,29).

The current research is an approach at a novel bulking agent which would be integrated into the tissue, therefore migration (30) would be avoided and urethral augmentation would be achieved.

1.2 Research Objectives

a) Design, fabricate, and characterize a material to create a transient immune response and tissue augmentation

    Macroporous for tissue integration and augmentation

    Injectable for minimally invasive delivery of the material

    Bioactive coating for a transient immune response

b) Create an *in vitro* model for investigating the immune response of the bioactive material by use of a three dimensional co-culture system

    Use a bioactive material with a known response *in vivo* and measure cytokine expression to show specific immune response

    Cell-cell interaction – how the co-culture affects their interaction and if this is reflective to the *in vivo* environment

c) *In vivo* testing of novel biomaterial

    Cell infiltration – tissue integration

    Inflammatory response – foreign body reaction

    Blood vessel infiltration – tissue integration

    ECM deposition – healing around implanted material

The above research objectives will be discussed in the following chapters. Chapter two will discuss the material fabrication and characterization. Chapter three will show the *in vitro* response of the bioactive coating. Chapter four will show a proof-of-concept murine subdermal implantation of the material and the resulting effects. Chapter five will discuss future directions and potential clinical applications for the material and give one example of a rodent experiment with a periurethal bulking model for urinary incontinence.

1.3 References

1. Elias CN, Lima JHC, Valiev R, Meyers MA. Biomedical applications of titanium and its alloys. JOM. 2008 Mar 1;60(3):46–9.

2. Williams DF. On the mechanisms of biocompatibility. Biomaterials. 2008 Jul;29(20):2941–53.
3. Hanks CT, Wataha JC, Sun Z. In vitro models of biocompatibility: A review. Dent Mater. 1996 May;12(3):186–93.
4. Zhang L, Zhou L, Xue Z. [Influence of fibrin glue on biliointestinal anastomotic scar formation]. Zhonghua Wai Ke Za Zhi. 1997 Mar;35(3):186–8.
5. Puri N, Talwar A. The Efficacy of Silicone Gel for the Treatment of Hypertrophic Scars and Keloids. J Cutan Aesthetic Surg. 2009;2(2):104–6.
6. Scar Revision Treatment & Management. 2012 Sep 17 [cited 2013 Oct 10]; Available from: http://emedicine.medscape.com/article/1129913-treatment
7. Lemperle G, Romano JJ, Busso M. Soft Tissue Augmentation With Artecoll: 10-Year History,Indications, Techniques, and Complications. Dermatol Surg. 2003;29(6):573–87.
8. Hanke CW, Higley HR, Jolivette DM, Swanson NA, Stegman SJ. Abscess formation and local necrosis after treatment with Zyderm or Zyplast Collagen Implant. J Am Acad Dermatol. 1991 Aug;25(2, Part 1):319–26.
9. Moon LDF, Fawcett JW. Reduction in CNS scar formation without concomitant increase in axon regeneration following treatment of adult rat brain with a combination of antibodies to TGFβ1 and β2. Eur J Neurosci. 2001;14(10):1667–77.
10. Shah M, Foreman DM, Ferguson MW. Neutralisation of TGF-beta 1 and TGF-beta 2 or exogenous addition of TGF-beta 3 to cutaneous rat wounds reduces scarring. J Cell Sci. 1995 Mar 1;108(3):985–1002.
11. Wilgus TA, Vodovotz Y, Vittadini E, Clubbs EA, Oberyszyn TM. Reduction of scar formation in full-thickness wounds with topical celecoxib treatment. Wound Repair Regen. 2003;11(1):25–34.

12. Li Z, Bergen TV, Veire SV de, Vel IV de, Moreau H, Dewerchin M, et al. Inhibition of Vascular Endothelial Growth Factor Reduces Scar Formation after Glaucoma Filtration Surgery. Invest Ophthalmol Vis Sci. 2009 Nov 1;50(11):5217–25.
13. Molyneux AJ, Kerr RS, Yu L-M, Clarke M, Sneade M, Yarnold JA, et al. International subarachnoid aneurysm trial (ISAT) of neurosurgical clipping versus endovascular coiling in 2143 patients with ruptured intracranial aneurysms: a randomised comparison of effects on survival, dependency, seizures, rebleeding, subgroups, and aneurysm occlusion. The Lancet. 3;366(9488):809–17.
14. Murayama Y, Tateshima S, Gonzalez NR, Vinuela F. Matrix and Bioabsorbable Polymeric Coils Accelerate Healing of Intracranial Aneurysms Long-Term Experimental Study. Stroke. 2003 Aug 1;34(8):2031–7.
15. Murayama Y, Viñuela F, Tateshima S, Gonzalez NR, Song JK, Mahdavieh H, et al. Cellular Responses of Bioabsorbable Polymeric Material and Guglielmi Detachable Coil in Experimental Aneurysms. Stroke. 2002 Apr 1;33(4):1120–8.
16. Page RC, Eke PI. Case definitions for use in population-based surveillance of periodontitis. J Periodontol. 2007 Jul;78(7 Suppl):1387–99.
17. Zetu L, Wang H-L. Management of inter-dental/inter-implant papilla. J Clin Periodontol. 2005 Jul;32(7):831–9.
18. Roman A, Louise F, M'barek R, Brunel-Trotebas S. Gingival Recessions: Epidemiologic, Etiologic and Therapeutic Aspects. Internet J Dent Sci. 2009;7(1):9.
19. Albandar JM, Kingman A. Gingival recession, gingival bleeding, and dental calculus in adults 30 years of age and older in the United States, 1988-1994. J Periodontol. 1999 Jan;70(1):30–43.

20. Nordland WP, Sandhu HS, Perio C. Microsurgical technique for augmentation of the interdental papilla: three case reports. Int J Periodontics Restorative Dent. 2008 Dec;28(6):543–9.
21. K Kotsilkov CP. THE APPLICATION OF A MINIMAL INVASIVE CONNECTIVE TISSUE GRAFT TECHNIQUE (ENVELOPE TECHNIQUE) IN A TREATMENT OF A GINGIVAL …. J IMAB. 2008;2:16–8.
22. Moharamzadeh K, Brook IM, Van Noort R, Scutt AM, Thornhill MH. Tissue-engineered oral mucosa: a review of the scientific literature. J Dent Res. 2007 Feb;86(2):115–24.
23. Tal H. Subgingival acellular dermal matrix allograft for the treatment of gingival recession: a case report. J Periodontol. 1999 Sep;70(9):1118–24.
24. Shanmugam M, Sivakumar V, Anitha V, Sivakumar B. Clinical evaluation of alloderm for root coverage and colour match. J Indian Soc Periodontol. 2012 Apr;16(2):218–23.
25. Norton P, Brubaker L. Urinary incontinence in women. The Lancet. 7;367(9504):57–67.
26. Rogers RG. Urinary Stress Incontinence in Women. N Engl J Med. 2008;358(10):1029–36.
27. Serati M, Salvatore S, Uccella S, Artibani W, Novara G, Cardozo L, et al. Surgical treatment for female stress urinary incontinence: what is the gold-standard procedure? Int Urogynecology J. 2009 Jun 1;20(6):619–21.
28. Lightner DJ. Review of the available urethral bulking agents. Curr Opin Urol. 2002 Jul;12(4):333–8.
29. McGuire EJ. Urethral bulking agents. Nat Clin Pract Urol. 2006;3(5):234–5.
30. Dmochowski RR, Appell RA. Injectable agents in the treatment of stress urinary incontinence in women: where are we now? Urology. 2000 Dec;56(6, Supplement 1):32–40.

CHAPTER TWO

DESIGNING MACROPOROUS MICROPARTICLES FOR SOFT TISSUE AUGMENTATION

The parameters for designing a material for this project were very specific. There needed to be a two component system. The first component is a bioactive layer which serves the purpose of eliciting a localized immune response, but this material then must degrade (within days *in vivo*), so the tissue can regain homeostasis. The second component has to have enough structural stability to augment the tissue for an extended period of time, enough hydrophilicity to allow for a low antigenic response, and enough porosity to allow for tissue in-growth to anchor the material. Together the two materials needed to be of a shape and size which is easily deliverable via needle injection and will not cause frustrated phagocytosis nor lead to a chronic inflammatory response.

2.1 Injectable Macroporous Microparticles for Soft Tissue Augmentation

2.1.1 Introduction

Synthetic polymers are used to make scaffolds for biomedical engineering applications because they are biocompatible and easily modified for specific applications. However, synthetic polymers have a lack of porosity due to the formation of long, inter-twining polymer chains. Without interconnecting pores, the body cannot sufficiently interact with the material and integrate the material into the existing tissue (1). In addition to the lack of porosity, the size of typical implants make them difficult to modify for soft tissue augmentation and subcutaneous injection. Synthetic polymer scaffolds typically require an invasive surgical procedure to be implanted which causes extended healing times and scar formation. To reduce the invasive-

ness of a typical procedure, materials which can be miniaturized for injection would be optimal. Therefore, there is a need for a macroporous, injectable scaffold system which can be tailored to meet the specifications of biological applications.

Macroporous scaffolds have been developed as a way to promote cell infiltration and integration with the existing tissue. Porous scaffolds have been fabricated using various techniques including particulate leaching, gas foaming, and solid freeform fabrication (2). Particulate leaching can be achieved using a salt or sugar particle of a specific size. This process combined with sufficient packing density can yield a highly porous structure (3). Gas foaming is aided by the use of an effervescent salt which creates gas bubbles upon contact with an appropriate solvent (4). Three-dimensional printing utilizes solid freeform fabrication as a means to make a porous structure by polymer infiltration after a three-dimensional model has been created. The goal of these techniques is to create interconnecting pores that allow cell infiltration and subsequent matrix deposition throughout the scaffold. The drawback to these porous, polymeric scaffolds is their large size and that they must be implanted with a surgical procedure.

To overcome these limitations, researchers have developed techniques to fabricate polymer scaffolds which are small enough to inject. This has been achieved using emulsion techniques to create microparticles (5). Microparticles can be easily injected and have been used for many applications including drug delivery and dermal augmentation (6,7). By manipulation of the processing parameters during fabrication, microparticles of varying size and structure can be created which provide temporal control over the interaction with the body (8). Currently strategies to create porous microparticles result in nanopores on the surface of the particles (9,10). The small pore size could be useful for drug delivery or diffusion through the pores, however, nano-sized pores do not allow cell infiltration. Fabrication of macroporous microparticles has been investigated by various groups, however most are created using

complex processes which are not viable in a simple lab setting (11–14). To maximize the utility of macroporous microparticles, there is a need for a simple, reproducible method to achieve large, highly interconnected surface and interior pores. There are many potential benefits to the fabrication of a macroporous scaffold which has the versatility of being injectable.

Biomaterials have been extensively studied with the ultimate goal during fabrication and testing being to achieve the most inert, biocompatible material possible (15). The biocompatibility of a material which is to be implanted is tested for cell attachment, proliferation and differentiation. If a material is cytotoxic it is considered to be non-biocompatible (16). When tested in vivo, the desirable effect of a material is a non-effect. A non-effect means that a material should have good tissue integration and not have a significant inflammatory response. Microparticles are often used because their smaller size can lead to less frustrated phagocytosis and more tissue integration in the body.

This study focuses on combining the benefits of both the particulate leaching/gas foaming technique and the microemulsion technique to create macroporous microparticles as an injectable polymer scaffold system. To the best of our knowledge, this is the first study which demonstrates a simple procedure to obtain macroporous polymer microparticles which subsequently exhibit optimal tissue integration through the interconnected pores of the microparticles.

2.1.2 Materials and Methods

A. *Materials*

Poly (ε-caprolactone) (PCL), Mn 70,000-90,000 and polyvinyl alcohol (PVA), Mw 31,000-50,000, 98-99% hydrolyzed were purchased from Sigma (St. Louis, MO). Dichloromethane (DCM) was obtained from Acros Organics. Ammonium bicarbonate was purchased from Fisher Scientific (Pittsburgh, PA).

B. *Preparation of Macroporous Microparticles*

Macroporous microparticles were fabricated with a water/oil/water (W/O/W) double emulsion method. PCL (200mg) was dissoluted in 3mL of dichloromethane overnight. Varying amounts of ammonium bicarbonate in 1mL nanopure water were added to the polymer solution and the resulting emulsion was vortexed for 2 minutes. Immediately following the vortexing, the primary emulsion was poured into a beaker containing 125mL of 0.1% (w/v) PVA solution. This second emulsion was then spun for 2 hours at 400rpm and 30°C to allow the solvent to evaporate. The resulting macroporous microparticles were washed 3 times with nanopure water to remove excess PVA solution. Finally, the particles were lyophilized with a freeze dryer overnight.

C. *Characterization of Microparticles*

Freeze dried microparticles were visualized using a scanning electron microscope. Particle sizes were analyzed on Image J software (US National Institute of Health). Surface porosity and interconnectivity were performed using threshold intensity of pixels in scanning electron micrographs using ImageJ software. The internal pores were visualized by embedding the PCL microparticles in Optimum Cutting Temperature (O.C.T.) solution, freezing the samples at -80°C, then having them processed by cutting 10μm slices on a microtome. The slides were imaged using optical microscopy. The surface roughness of the microparticles was characterized using MeX software with stereo imaging on the scanning electron microscope.

D. *Microparticles in a Murine Model*

C57BL/6 mice (age 10-13 weeks) were purchased from Charles River Laboratories, Wilmington, MA. The animals were handled in compliance with the institutional regulations established and approved by the Animal Research Committee at the University of California, Los Angeles. For scaffold implantation, mice were anesthetized with isofluorane and a 1-cm long dorsal midline incision was made to create a subcutaneous pocket. A thin (~200μm), laser-cut PCL sheet was rolled into a tube and filled with macroporous microparticles then inserted in the subcutaneous

pocket about a centimeter away from the incision, and the skin was sutured with 3-0 Vicryl (Ethicon, Somerville, NJ). One scaffold was implanted in each mouse.

The animals were sacrificed at 7 and 14 days post-implantation. The scaffolds, along with the adjacent subcutaneous tissue, were harvested and fixed promptly in 10% formalin overnight at 4°C.

E. *Immunohistochemistry*

The fixed samples were embedded in paraffin and sectioned at 6 μm. The deparaffinized sections were stained with hematoxylin and eosin. Hematoxylin and eosin (H&E) sections were used to verify overall cell infiltration and tissue integration of the PCL microparticles.

2.1.3 Results and Discussion

Microparticles fabricated using a double emulsion technique with an effervescent salt were macroporous and had a range or particle sizes with consistent interconnected pores. The W/O/W emulsion had ammonium bicarbonate in the W1 phase to create the pores, PCL dissolved in dichloromethane as the O phase, and 0.1% PVA as the W2 phase. The W1 and O phase was vortexed to achieve the primary emulsion which was then poured into the W2 phase and re-emulsified resulting in microparticles. Bubbles of carbon dioxide and ammonia gases are formed when the ammonium bicarbonate comes into contact with water. These gas bubbles leave voids in the polymerizing microparticle as the oil-based solvent evaporates in the secondary emulsion. This process results in the creation of macropores in the microparticles. Unlike similar techniques for macroporous microparticles, our technique gives interconnectivity of pores through the combined particulate leaching/ gas foaming technique. The interconnectivity of surface pores and the size of internal pores were examined with scanning electron microscopy and cryo-sectioning. Pore size range was large with an average pore size of ~20 μm.

Table 2-1 – Size of PCL Microparticles				
NH_4HCO_3	*Spin Speed*	*Microparticle Diameter*	*Average Pore Diameter*	*% Area Porous*
0%	400 RPM	128± 57 µm	-	-
5%	400 RPM	338± 90 µm	11.9 µm	19.90%
10%	400 RPM	384± 86 µm	10.7 µm	24.20%
20%	400 RPM	465± 95 µm	10.2 µm	16.90%
40%	200 RPM	1003 ± 330 µm	12.0 µm	20.10%
40%	400 RPM	520 ± 79 µm	10.0 µm	17.70%
40%	600 RPM	*shredded	-	-

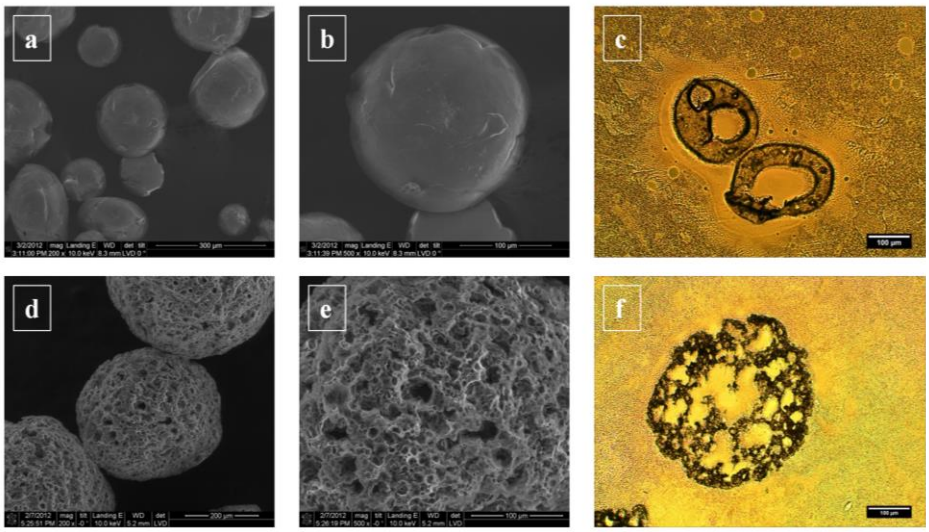

Figure 2-1. **a-c** PCL microparticles with 0% ammonium bicarbonate.

d-f PCL macroporous microparticles with 40% ammonium bicarbonate. **a, d** Gross morphology of microparticles 200X on SEM. **b, e** Surface morphology of microparticles 500X on SEM. **c, f** 10um cross-sections from cryo-sectioned microparticles, 100um scale bar.

These particles and pores sizes were modulated by altering the material processing parameters. PCL macroporous microparticles had larger sizes at both slower spin speeds and higher concentrations of ammonium bicarbonate (Table 2-1). The gross morphology as well as the surface morphology and the cross-sectioned slices of particles show the qualitative difference seen with addition of the effervescent salt to the double emulsion technique (Fig. 2-1). When there was an absence of ammonium bicarbonate, the resultant microparticles had a smoother texture and much smaller particle diameters. This data shows that as the percent ammonium bicarbonate was increased, the overall size distribution of particles also increased. A typical histogram of particle size distribution can be seen in fig. 2-2, with a summary of size distribution in table 2-1. The effect of the ammonium bicarbonate producing gaseous bubbles in the primary emulsion causes the increase in particle diameter. As the percent of ammonium bicarbonate increases, so does the number of gas bubbles formed. The pressure the bubbles produce pushes against the polymer as the solvent evaporates, therefore enlarging the microparticles as they are formed. As the polymer phase is solidifying (due to dichloromethane evaporation) and viscosity is increasing, the bubbles create less stress on the polymer as it stiffens and the gas phase eventually escapes through the interconnecting pores. Surface and interior pore sizes, as well as percentage of surface pores interconnected remain consistent throughout most processing parameters (Table 2-1, Fig. 2-2). The gaseous bubbles surrounding the microparticles as they form, prevents the coalescence of particles. This emulsion is achieved without addition of surfactants due to the stabilization that the gas bubbles have on the microemulsion (14). Without the gas formation, particles would be less stable in the material fabrication process leading to aggregation of polymer microparticles.

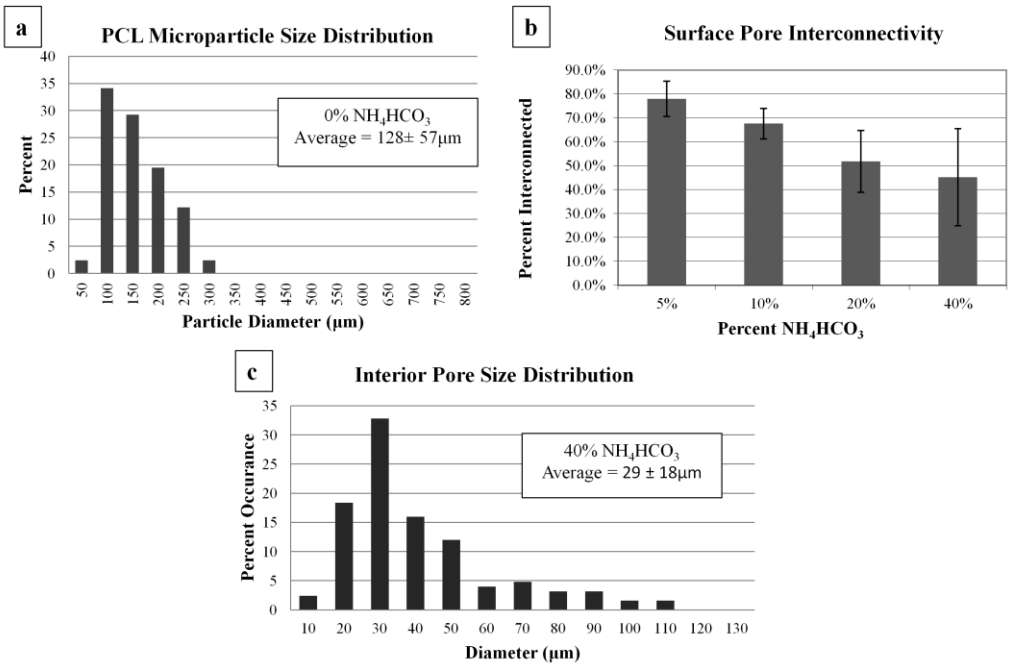

Figure 2-2. a. Typical histogram of PCL microparticle size distribution **b.** Surface Pore Interconnectivity with varying concentrations of ammonium bicarbonate **c.** Internal Porosity of microparticles made with 40% NH_4HCO_3

SEM image analysis on micrographs of the PCL microparticles results in an average particle size of 128± 57 μm, 338± 90 μm, 384± 86 μm, 465± 95 μm, and 520 ± 79 μm with a concentration of 0%, 5%, 10%, 20%, and 40% ammonium bicarbonate, respectively. Surface pore sizes for the microparticles averaged 10 ±1 μm for each of the sets with ammonium bicarbonate (Table 2-1). Interior pore diameters averaged to be 29 ± 18 μm when visualized by 10 μm slices of cryo-sectioned particles (Fig. 2-1, Fig. 2-2). When the percent ammonium bicarbonate was altered, there was no significant change in particle morphology, however, the surface roughness decreases with increases in ammonium bicarbonate (unpublished data). This follows with the small decrease in surface pore size seen with the addition of ammonium bicarbonate.

The *in vivo* response to the PCL macroporous microparticles has been investigated. Small packets of microparticles in a PCL pouch were implanted subcutaneously in a mouse model. A representative explant can be seen in fig. 2-3. The microparticles were implanted and not injected to fully immobilize the particles, however, subcutaneous injection is possible and was performed in a few animals (Fig. 2-3a). Upon harvest of the polymer microparticles and surrounding tissue, immunohistochemistry was performed to analyze cell/tissue infiltration/integration, as well as blood vessel formation throughout the PCL microparticles. From the H&E stained slides shown in fig. 2-3, it is apparent that there is some cell infiltration at day 7, however, by day 14 there is blood vessel formation and more tissue integration. The ability of the microparticles to integrate into the existing tissue is due to the size and interconnectivity of the pores. With high levels of tissue integration, there is improved acceptance of the material into the body and the ability for soft tissue augmentation without significant inflammation. This response is desirable and applicable in a variety of medical fields including dentistry and dermatology.

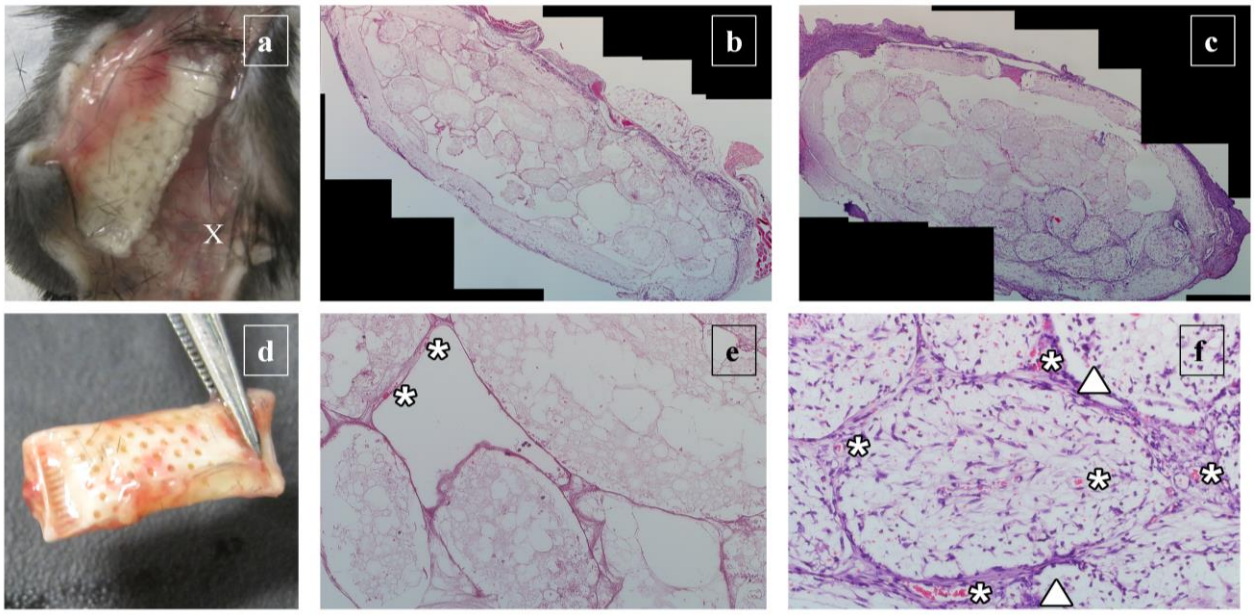

Figure 2-3. **a, d.** Typical explants of PCL pockets filled with microparticles at one week post implantation. **X** indicates where macroporous PCL microparticles can be seen when injected adjacent to a PCL pocket implant. **b, e.** H&E staining of paraffin sections of one week implants. **c, f.** H&E staining of paraffin sections of two week implants. ***** denotes blood vessels. **Δ** denotes areas of foreign body giant cell formation

2.1.4 Conclusion

The fabrication of macroporous PCL microparticles establishes a simple material processing technique which can be utilized as an injectable polymer system. The combination of gas foaming and particulate leaching achieved polymer microparticles with interconnected pores which allowed for tissue in-growth upon implantation. The versatility of application for this technology spans many areas of biomedical engineering.

2.2 Macroporous PCL Microparticles – Changing the Dimensions

2.2.1 Materials and Methods

Macroporous PCL Microparticles

PCL microparticles were fabricated according to the previous protocol (17), however, there were alterations made to the weight percent polymer in the emulsion solution. Additionally, the percentage of ammonium bicarbonate was varied to obtain different particle sizes as well.

Scanning electron microscopy was used to image the particle surfaces and the resulting images were used to calculate particle size, pore size, and percent area porous.

2.2.2 Results

Macroporous PCL microparticles can be fabricated with a wide range of sizes (Table 2-1 and Table 2-2) from about 100µm to 1000µm with altering the materials processing parameters. The particles have similar surface pore sizes (~10-12µm) across the entire size range. The percent area porous appears to increase with increasing polymer weight percent. The macroporous PCL microparticles are very reproducible and have a small size distribution within each set.

The particle fabrication process includes multiple steps which have effects on the outcome of the particles. The addition of ammonium bicarbonate in water to the PCL in DCM of the primary emulsion allows for the gas foaming process to begin. The gases formed are carbon dioxide and ammonia. As these gases begin to form in the primary emulsion, the polymer is in the liquid state (Figure 2-4b). Once the primary emulsion is poured into the spinning PVA solution, the porous particles begin to form and the polymer transitions from the liquid to the sol-gel state (Fig. 2-4c). Without the effervescent salt, a traditional double emulsion technique results in one large pore in the interior of the microparticles (Figure 2-1) due to the water phase merging in the primary emulsion. In the current gas foaming technique with the

addition of ammonium bicarbonate as an effervescent salt, gas bubbles form around the water droplets in the primary emulsion stabilizing the water droplets and preventing them from joining. This creates a homogeneous distribution of small water droplets and forming gas bubbles within the primary emulsion. Following gas bubble formation and transfer into the secondary emulsion, the gas bubbles are now forming within the interior of each particle and they coalesce and transverse their way to escape at the surface of the forming particle as the polymer is in the sol-gel state. It is hypothesized that the consistent temperature and pH conditions of the spinning PVA in the secondary emulsion, results in the similar sized surface pores for the macroporous PCL microparticles (Table 2-1 and 2-2). Therefore, these fabrication parameters could potentially be altered to obtain even a wider size range of particles or varied pore sizes.

For example if the processing parameters were kept constant, but the secondary emulsion was carried out at an elevated temperature, the solvent would evaporate from the emulsion more quickly resulting in smaller particles with potentially lower percent area porous on the surface. This would result because the polymer would transition from the rubbery, sol-gel state to the glassy state much more quickly in the elevated temperature due to the accelerated solvent evaporation. Alternately, if the fabrication was carried out in a closed system of a pressurized vessel, the gassing out of the ammonia and carbon dioxide would likely happen on a slower time scale resulting in larger interior porosity due to the coalescence of more gas bubbles before they reach the surface of the forming particle. This could potentially result in larger surface porosity as well as larger particle formation.

In addition to altering the processing parameters to achieve various particle formation, it was found that the PVA selection also had a tremendous effect on the formation of the macroporous PCL microparticles. With an 87-89% hydrolyzed formula of PVA, nice, even porous particles are achieved. However, if 98-99% or 99%+ hydrolyzed PVA are used, no porous particles are formed (data not shown). The difference in the PVA types is their acetate

content. The 87-89% hydrolyzed PVA contains about 12% acetate. The acetate groups act as spacers between the PVA chains. Without the acetate spacers (or having significantly fewer acetate spacers), as with the 98-99% and 99%+, the PVA becomes extremely hydrogen bonded to itself. When the PCL solution is added to the high hydrolysis PVA chains, it results in one large hunk of polymer instead of discreet particles due to the hydrophobicity of PCL (data not shown). This result stresses the need for very specific and consistent processing parameters to achieve the macroporous PCL microparticles.

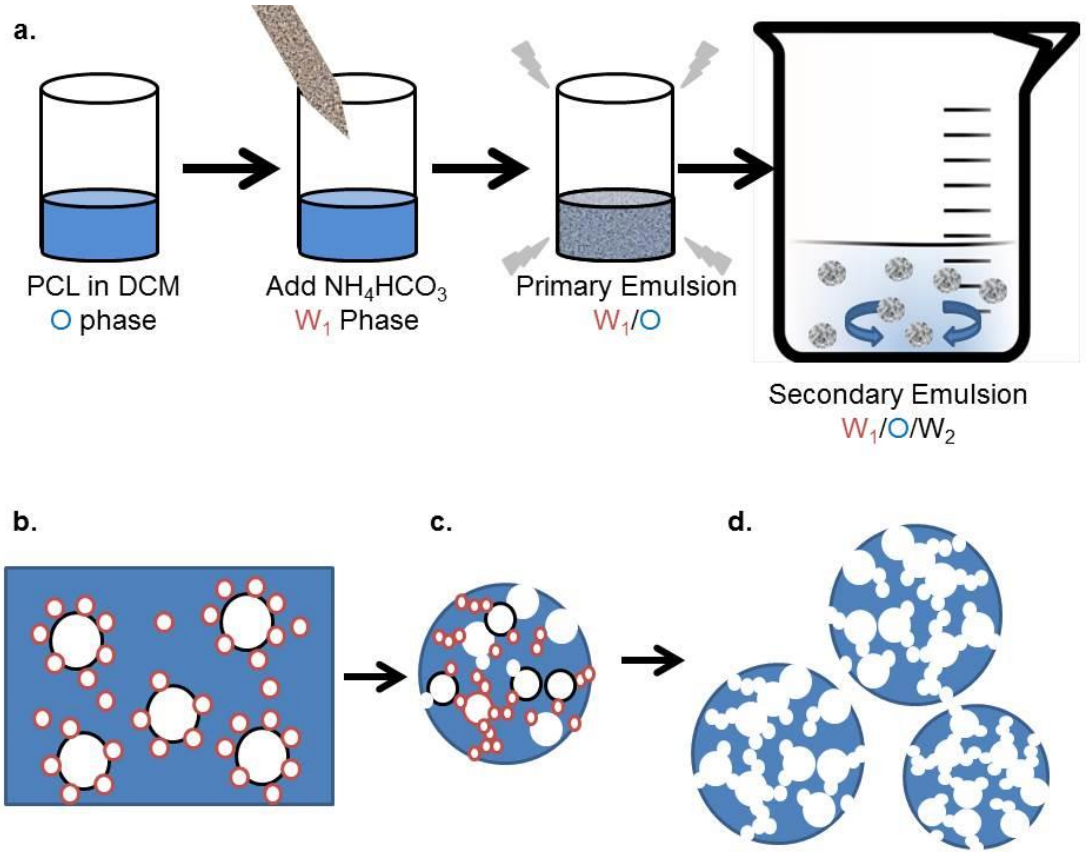

Figure 2-4. Schematic of the Macroporous PCL microparticle fabrication process **a.** Schematic of the fabrication process. **b**. In the primary emulsion, small ammonia and carbon dioxide gas bubbles evolve from the water droplets and may sterically prevent water droplets from coalescing, which reduces the interfacial area between phases. **c.** In the secondary emulsion, gas bubbles continue to be released from the ammonium bicarbonate decomposing along with the solvent evaporation, and this process of the gas formation should set to form porous structure within the microsphere and porosity on the surface where the gas bubbles escape. **d.** Final porous structure of the macroporous PCL microspheres.

Table 2-2 - Size of PCL Microparticles				
PCL wt %	*NH_4HCO_3*	*Microparticle Diameter (µm)*	*Pore Diameter*	*% Area Porous*
1	10%	73.2 ± 11	9.8 µm	11.16
2	10%	140.2 ± 28	11.7 µm	14.76
3	10%	209 ± 39	11.3 µm	17.58
5	10%	272 ± 66	11.6 µm	20.68
6.67	5%	338.6 ± 90	11.9 µm	19.90
6.67	10%	385 ± 86	10.7 µm	24.20
6.67	20%	465 ± 95	10.2 µm	16.90
6.67	40%	520 ± 79	10.0 µm	17.70

Table 2-2 Size of PCL microparticles with altering the polymer concentration and the percentage of ammonium bicarbonate.

2.2.3 Discussion

The advantage to creating macroporous PCL microparticles of different sizes is evident in the clinical applications. With a wide variety of sizes, the application potential grows as well. Different soft tissue defect sizes can be addressed with the particle size ranges fabricated. Additionally, the smaller size particles can easily be administered via small gauge needle injection. This minimally invasive delivery is preferential in a growing medical field because it allows for a quick delivery, administrator ease of use, and an increase in patient comfort over traditional surgeries. Additionally, small size, porous bulking materials allow for cell and blood vessel infiltration resulting in anchoring of a material due to the increase in cells and sustainability of the cells due to the blood vessel vicinity. Blood vessels must be within 200µm of the surface of a vessel in order to exchange oxygen and nutrients (18). The smaller size particles, allow for this limited distance to be achieved in and around the actual particles themselves.

The potential applications for macroporous microparticles include filler and bulking uses. These applications span the fields of dermatology, urology, gastroenterology, and dentistry. A potential dermalogical application is as an injectable for soft tissue filler. The advantage to macroporous PCL microparticles is that we believe they will have a longer life span *in vivo* than most liquid dermal injectables (19,20) and a more acute inflammatory response than existing dermal filler particles fabricated out of PMMA (7,21,22) which result in chronic inflammation. In the field of urology, urinary incontinence can be a negative life changing experience for a patient. Macroporous PCL microparticles could be delivered as a periurethral bulking agent which could help the musculature regain control. Previously, solid PCL particles have been demonstrated subcutaneously as a potential bulking agent (23) and we believe that the macroporous PCL microparticles offer a significant advantage in that cells can infiltrate the particles which can result in better tissue integration (17). Gastroenterology has sphincter

bulking applications for the PCL microparticles. Sphincter bulking can help control gastroesophageal reflux disease (GERD) (24) and bring comfort to patients. In dentistry, gingival recession is a problem in 58% of the population 30 years and older (25). The current surgery for correction is an envelope procedure where tissue from the upper palate is harvested and implanted in a gingival envelope, then closed with sutures (26,27). The recovery time can be months from this surgery, therefore a minimally invasive injection, such as that of macroporous PCL microparticles is advantageous to the patient.

Other groups have created macroporous microparticles (14,28–32), however they have drawbacks when it comes to implementing clinical applications. Silk fibroin particles have been used to attempt to demonstrate use of an alternative material as a cell carrier, however, after 8 weeks *in vivo* there is not complete cell infiltration into the particles (31). PLGA has been fabricated into porous microspheres with a gas foaming technique (14,29), however, PLGA is a short-lived material *in vivo* which makes it undesirable as a long-term bulking agent for tissue augmentation. Additionally, they do not demonstrate particle or pore size variability with their processing parameters and their conditions sometimes result in closed surface pores instead of interconnected porosity. To increase the duration *in vivo* the material can be changed to something such as PCL. PCL has been used with a melt-molding thermal compression method to obtain macroporous particles (32), however this fabrication technique is complicated and a very long, involved process.

The macroporous PCL microparticles fabricated in this research have many potential clinical applications within tissue augmentation and many advantages over existing therapies. The extensive size range (100µm - 1000µm) that is able to be fabricated with altering the materials processing parameters (spin speed, percent effervescent salt, and polymer concentration) adds to the utilization of these particles. The control over size range is achieved while still maintaining macroporosity on the surface of the microparticles. This porosity allows

for cell infiltration and potential tissue integration once implanted. PCL is known to last for years *in vivo* (33) however it does not persist permanently as to avoid a chronic foreign body response. Additionally, PCL itself has many advantages including previous FDA approval for various implants that incorporate the polymer (34) and the longevity of the material *in vivo* (33,35).

2.3 Bioactive PLGA Coating onto Macroporous PCL Microparticles

2.3.1 Introduction

In previous applications, poly lactic co-glycolic acid (PLGA) has been shown to increase collagen deposition, therefore decreasing healing time (36). With this in mind, it was hypothesized that with the introduction of PLGA to our macroporous particle system, we would obtain faster cell infiltration and subsequent extracellular matrix deposition and tissue integration.

2.3.2 Materials and Methods

Spray coating the macroporous PCL microparticles was performed using a pressurized spray gun system. The microparticles were sandwiched between two sieves. A 1% solution of PLGA (Lakeshore Biomaterials) in acetone (Fisher Scientific) (wt/vol) was then atomized with 20psi and deposited on the surface of the PCL particles.

To ensure even coating, calcium chloride (Sigma-Aldrich) in ethanol (Sigma-Aldrich) was mixed with the PLGA in acetone spray solution. This allowed for the use of spectral elemental analysis within the scanning electron microscope (SEM-EDS) to be performed which indicated the spatial and quantitative distribution of calcium and chloride. The locations of calcium and chloride also should indicate where the PLGA is deposited.

2.3.3 Results

The atomized spray technique allows for deposition of a thin layer of PLGA onto the surface of the macroporous PCL microparticles. This thin coating will allow for the potential bioactive properties of PLGA to be localized at the surface of the polymer struts of the microparticles, resulting in a localized response. Figure 2-5 shows spectral distribution of carbon, oxygen, calcium and chloride on the surface of the PCL macroporous microparticles. Figure 2-6 is the quantitative analysis of the spectral distributions obtained from the SEM-EDS.

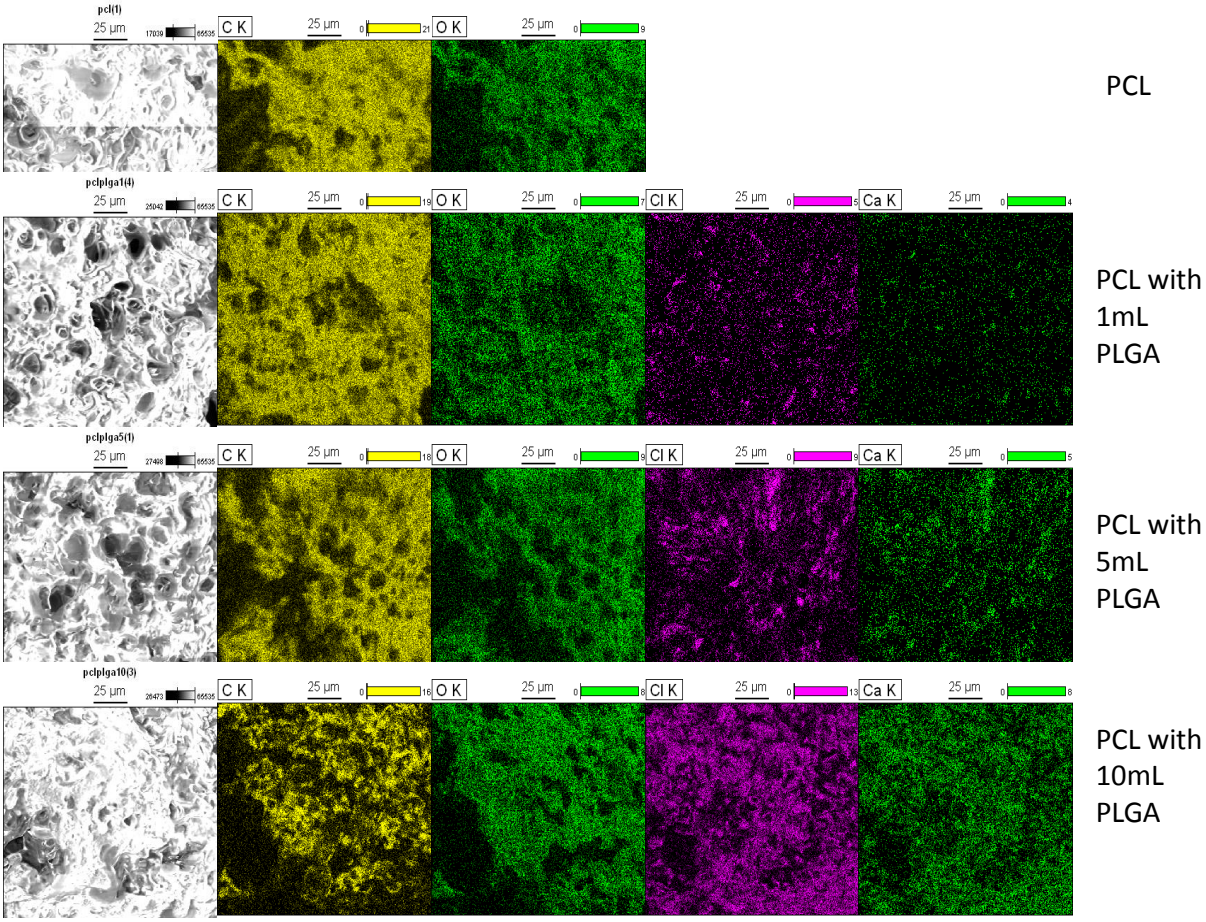

Figure 2-5

SEM-EDS analysis of the surface of macroporous PCL microparticles spray coated in a calcium chloride/ PLGA solution. Scale bar = 25µm.

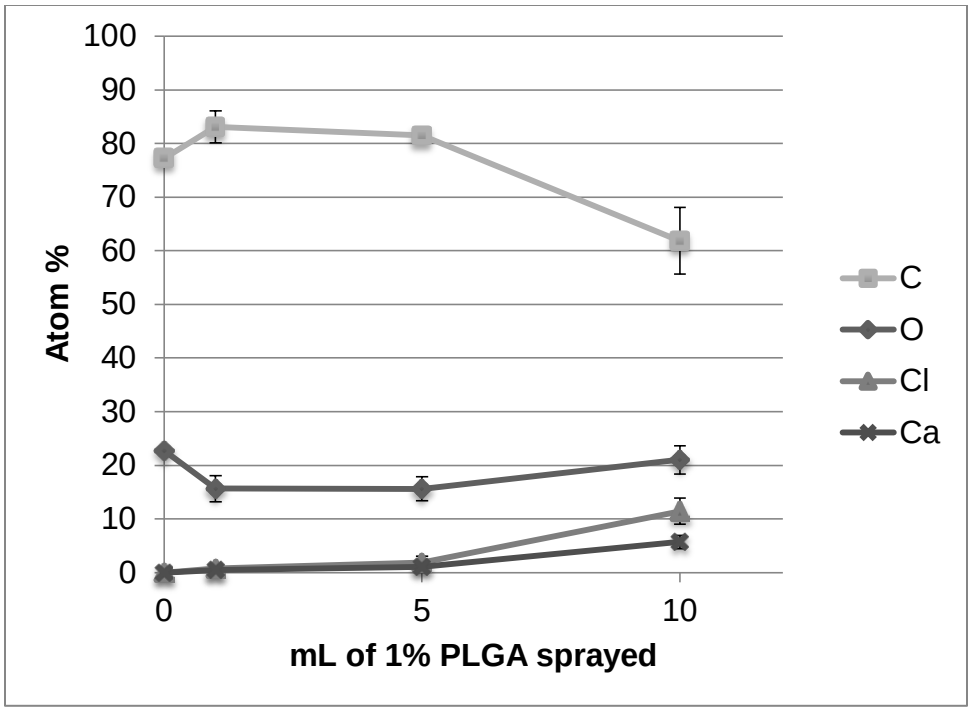

Figure 2-6

Atom percent of macroporous PCL microparticles spray coated in a calcium chloride/ PLGA solution

2.3.4 Discussion

The distribution of the PLGA (Fig. 2-5) is an even coating on the surface of the macroporous PCL microparticles. As the sprayed volume of $CaCl_2$ /PLGA solution is increased, the atom percent of both calcium and chloride increase on the surface of the particles (Fig. 2-6). This coating response is evidence that we are able to obtain an even coating of the spray solution and a thicker layer with the larger volume sprayed.

2.4 References

1. Carrubba V, Pavia FC, Brucato V, Piccarolo S. PLLA/PLA scaffolds prepared via Thermally Induced Phase Separation (TIPS): tuning of properties and biodegradability. Int J Mater Form. 2008 Apr 17;1(S1):619–22.
2. Taboas J., Maddox R., Krebsbach P., Hollister S. Indirect solid free form fabrication of local and global porous, biomimetic and composite 3D polymer-ceramic scaffolds. Biomaterials. 2003 Jan;24(1):181–94.
3. Mikos AG, Temenoff JS. Formation of highly porous biodegradable scaffolds for tissue engineering. Electron J Biotechnol. 2000 Aug;3(2):23–4.
4. Yoon JJ, Park TG. Degradation behaviors of biodegradable macroporous scaffolds prepared by gas foaming of effervescent salts. J Biomed Mater Res. 2001 Jun 5;55(3):401–8.
5. Freitas S, Merkle HP, Gander B. Microencapsulation by solvent extraction/evaporation: reviewing the state of the art of microsphere preparation process technology. J Controlled Release. 2005 Feb;102(2):313–32.
6. Siepmann J, Siepmann F. Microparticles Used as Drug Delivery Systems. In: Richtering W, editor. Smart Colloidal Materials [Internet]. Springer Berlin Heidelberg; [cited 2012 Mar 14]. p. 15–21. Available from: http://www.springerlink.com/index/10.1007/3-540-32702-9_3

7. Laeschke K. Biocompatibility of microparticles into soft tissue fillers. Semin Cutan Med Surg. 2004 Dec;23(4):214–7.
8. Norris DA, Sinko PJ. Effect of size, surface charge, and hydrophobicity on the translocation of polystyrene microspheres through gastrointestinal mucin. J Appl Polym Sci. 1997 Mar 14;63(11):1481–92.
9. Ehtezazi T, Washington C, Melia CD. First order release rate from porous PLA microspheres with limited exit holes on the exterior surface. J Control Release Off J Control Release Soc. 2000 May 3;66(1):27–38.
10. Sosnowski S, Woźniak P, Lewandowska-Szumieł M. Polyester Scaffolds with Bimodal Pore Size Distribution for Tissue Engineering. Macromol Biosci. 2006 Jun 16;6(6):425–34.
11. Hong S-J, Yu H-S, Kim H-W. Tissue Engineering Polymeric Microcarriers with Macroporous Morphology and Bone-Bioactive Surface. Macromol Biosci. 2009 Jul 7;9(7):639–45.
12. Davies OR, Marlow M, Stolnik S. Macroporous surface modified microparticles. Soft Matter. 2008;4(8):1597.
13. Straub JA, Chickering DE, Church CC, Shah B, Hanlon T, Bernstein H. Porous PLGA microparticles: AI-700, an intravenously administered ultrasound contrast agent for use in echocardiography. J Controlled Release. 2005 Nov;108(1):21–32.
14. Kim TK, Yoon JJ, Lee DS, Park TG. Gas foamed open porous biodegradable polymeric microspheres. Biomaterials. 2006 Jan;27(2):152–9.
15. Williams DF. On the mechanisms of biocompatibility. Biomaterials. 2008 Jul;29(20):2941–53.
16. Hanks CT, Wataha JC, Sun Z. In vitro models of biocompatibility: A review. Dent Mater. 1996 May;12(3):186–93.

17. Corrin AA, Ngai M, Walthers CM, Dunn JCY, Wu BM. Injectable macroporous microparticles for soft tissue augmentation. 2012 Annual International Conference of the IEEE Engineering in Medicine and Biology Society (EMBC). 2012. p. 2428 –2431.
18. Loffredo F, Lee RT. Therapeutic Vasculogenesis It Takes Two. Circ Res. 2008 Jul 18;103(2):128–30.
19. Teo EY, Ong S-Y, Khoon Chong MS, Zhang Z, Lu J, Moochhala S, et al. Polycaprolactone-based fused deposition modeled mesh for delivery of antibacterial agents to infected wounds. Biomaterials. 2011 Jan;32(1):279–87.
20. Dasaratha Dhanaraju M, Gopinath D, Rafiuddin Ahmed M, Jayakumar R, Vamsadhara C. Characterization of polymeric poly(ϵ-caprolactone) injectable implant delivery system for the controlled delivery of contraceptive steroids. J Biomed Mater Res A. 2006;76A(1):63–72.
21. Jones DH. Semipermanent and permanent injectable fillers. Dermatol Clin. 2009 Oct;27(4):433–444, vi.
22. Lemperle G, Romano JJ, Busso M. Soft Tissue Augmentation With Artecoll: 10-Year History,Indications, Techniques, and Complications. Dermatol Surg. 2003;29(6):573–87.
23. Oh SH, Lee JY, Ghil SH, Lee SS, Yuk SH, Lee JH. PCL microparticle-dispersed PLGA solution as a potential injectable urethral bulking agent. Biomaterials. 2006 Mar;27(9):1936–44.
24. Kamler JP, Lemperle G, Lemperle S, Lehman GA. Endoscopic lower esophageal sphincter bulking for the treatment of GERD: safety evaluation of injectable polymethylmethacrylate microspheres in miniature swine. Gastrointest Endosc. 2010 Aug;72(2):337–42.
25. Albandar JM, Kingman A. Gingival recession, gingival bleeding, and dental calculus in adults 30 years of age and older in the United States, 1988-1994. J Periodontol. 1999 Jan;70(1):30–43.

26. K Kotsilkov CP. THE APPLICATION OF A MINIMAL INVASIVE CONNECTIVE TISSUE GRAFT TECHNIQUE (ENVELOPE TECHNIQUE) IN A TREATMENT OF A GINGIVAL …. J IMAB. 2008;2:16–8.
27. Shanmugam M, Sivakumar V, Anitha V, Sivakumar B. Clinical evaluation of alloderm for root coverage and colour match. J Indian Soc Periodontol. 2012 Apr;16(2):218–23.
28. Maeng Y-J, Choi S-W, Kim HO, Kim J-H. Culture of human mesenchymal stem cells using electrosprayed porous chitosan microbeads. J Biomed Mater Res A. 2010 Mar 1;92(3):869–76.
29. Chung HJ, Kim IK, Kim TG, Park TG. Highly open porous biodegradable microcarriers: in vitro cultivation of chondrocytes for injectable delivery. Tissue Eng Part A. 2008 May;14(5):607–15.
30. Choi S-W, Yeh Y-C, Zhang Y, Sung H-W, Xia Y. Uniform beads with controllable pore sizes for biomedical applications. Small Weinh Bergstr Ger. 2010 Jul 19;6(14):1492–8.
31. Shi LB, Cai HX, Chen LK, Wu Y, Zhu SA, Gong XN, et al. Tissue engineered bulking agent with adipose-derived stem cells and silk fibroin microspheres for the treatment of intrinsic urethral sphincter deficiency. Biomaterials. 2014 Feb;35(5):1519–30.
32. Lim SM, Lee HJ, Oh SH, Kim JM, Lee JH. Novel fabrication of PCL porous beads for use as an injectable cell carrier system. J Biomed Mater Res B Appl Biomater. 2009 Aug;90(2):521–30.
33. Ma G, Song C, Sun H, Yang J, Leng X. A biodegradable levonorgestrel-releasing implant made of PCL/F68 compound as tested in rats and dogs. Contraception. 2006 Aug;74(2):141–7.
34. Woodruff MA, Hutmacher DW. The return of a forgotten polymer—Polycaprolactone in the 21st century. Prog Polym Sci. 2010 Oct;35(10):1217–56.

35. Darney PD, Monroe SE, Klaisle CM, Alvarado A. Clinical evaluation of the Capronor contraceptive implant: preliminary report. Am J Obstet Gynecol. 1989 May;160(5 Pt 2):1292–5.

36. Murayama Y, Viñuela F, Tateshima S, Gonzalez NR, Song JK, Mahdavieh H, et al. Cellular Responses of Bioabsorbable Polymeric Material and Guglielmi Detachable Coil in Experimental Aneurysms. Stroke. 2002 Apr 1;33(4):1120–8.

CHAPTER THREE

IN VITRO ANALYSIS OF BIOACTIVE PLGA – CO-CULTURE RESPONSE

3.1 Introduction

Wound healing around implants is orchestrated by cells and proteins of the immune system throughout the classical phases of inflammation, proliferation, and remodeling(1,2). A wide variety of biomaterials have been tested for their biocompatibility and their interaction with the immune system(3). Currently, *in vivo* animal models are the gold standard for evaluating biomaterial-host response, due to the scarcity of appropriate *in vitro* model systems that recapitulate physiological settings. However, the relative roles of cytokines and cell-material interactions during the inflammatory phases are difficult to study *in vivo* due to lack of specific control and high costs to study the large array of experimental variables(4,5). Furthermore, inter-species and individual variability preclude the development of personalized *in vivo* biocompatibility models that can predict patient-specific host response to a candidate device.

To address these needs, numerous *in vitro* two-dimensional (2D) model systems containing single (monoculture) and multiple (co-culture) cell-types with precise control over the experimental variables have been developed to study the inflammatory responses to biomaterials and are summarized in Table 1. Three-dimensional (3D) models have been proposed to offer a more natural cell morphology, adhesion pattern, migration, and cell function when compared to their 2D counterparts(6–9).

By offering tissue architecture and the cell-matrix, cell-cell interactions of 3D tissue microenvironment, 3D models have been proposed to be more physiologically relevant than 2D(9). 3D *in vitro* co-culture of hepatocytes and hepatic stellate cells mimic an *in vivo* hepatic environment and promoted the deposition of complex ECM support as well as a higher density of viable cells(10). In head to head comparison against 2D models, 3D cultures have been shown to offer better prediction of *in vivo* dose response to drugs(11), and more importantly,

greater detailed understanding of the 3D dose-response mechanism(12). 3D co-culture of human monocytes and endothelial cells under the proper conditions produced elevated levels of granulocyte macrophage colony-stimulating factor (GM-CSF) as seen during atherosclerosis(13,14).

To study material-cell response, several 3D hydrogels that provide tissue-like extracellular matrix (ECM) have been shown to promote optimal cell attachment and morphology(15–17). 3D co-cultures of mouse macrophages and fibroblasts in gelatin and alginate hydrogel constructs have demonstrated to be useful for measuring inflammatory factors(18). However, to the best of our knowledge, there are currently no reported 3D *in vitro* co-culture model systems to study soft tissue inflammatory responses using human cells, despite the merits of 3D co-culture models. Here we develop a 3D model to study the interaction between human cells and their surrounding matrix and implanted materials. Poly (lactic-co-glycolic acid) (PLGA) is used as a proto-typical, well characterized biomaterial to model the effects on human fibroblasts and activated monocytes in a 3D environment. This 3D *in vitro* co-culture model may have the cell types tailored to other tissues in the body to create alternative biomimetic environments and test materials or drugs. This method could potentially include a patient's own cells to predict personalized immunity to a material.

3.2 Materials and Methods

Cell culture and monocyte activation

Human foreskin fibroblasts (ATCC, Manassas, VA) were propagated in Dulbecco's Modification of Eagles Medium (DMEM) (Mediatech, Manassas, VA) supplemented with 10% Fetal Bovine Serum (FBS) (Omega Scientific, Tarzana, CA) and 1% Antibiotic-Antimycotic (Life Technologies, Carlsbad, CA) in a 37°C incubator with 5% CO_2. Human U937 Monocytes (ATCC, Manassas, VA) were cultured in RPMI-1640 (Mediatech, Manassas, VA) supplemented

with 10% FBS. The monocytes were activated using LPS (Sigma, St. Louis, MO) at a concentration of 100 ng/mL for four hours before use in the 3D *in vitro* culture.

Cell imaging and morphology analysis

To characterize monocyte activation, monocytes were stimulated with different concentrations of LPS: 0 µg/mL, 0.1 µg/mL, and 1 µg/mL and imaged on an optical microscope for size analysis with activation. Changes in cell dimensions and morphology were observed under phase contrast optical microscopy and analyzed using ImageJ software (NIH).

PLGA particle preparation and characterization

The PLGA particles were fabricated using a nano-precipitation method. Briefly, 3 mL of 6% (w/v) PLGA (Lakeshore Biomaterials, Birmingham, AL) in dichloromethane (DCM) (Sigma-Aldrich, St. Louis, MO) was prepared and put on an orbital shaker overnight to allow for dissolution. The following day an emulsion was prepared by pouring the PLGA/DCM solution into 200 mL of a 0.5% (w/v) poly-vinyl alcohol (PVA) (Sigma-Aldrich, St. Louis, MO) spinning at 600 rpm. After the 3 hours, the emulsion was removed from the magnetic stir plate and centrifuged at 3000 rpm to collect the particles. The PLGA was then washed three times with nanopure water and freeze-dried. The resulting particles were stored in -20°C.

The PLGA particles were characterized for size, morphology and degradation properties. The size and morphology were analyzed on a scanning electron microscope (SEM) (FEI Nova Nano 230) with a low vacuum detector. Since PLGA is known to release acidic products during degradation, solution pH was recorded on day 0, 1, 4, 7, and 10 during the biodegradation of 2.5 mg/mL PLGA microspheres in each degradation medium (water, RPMI, or collagen gel in RPMI).

In Vitro 3D Collagen Cell Culture System

The collagen hydrogel solution was made by mixing eight parts PureCol (Advanced Biomatrix, San Diego, CA) collagen, one part 10X RPMI (Sigma- Aldrich, St. Louis, MO), and

one part 0.1 N sodium hydroxide (Sigma- Aldrich, St. Louis, MO). The solution pH was adjusted to ~7.4 using 0.1 N sodium hydroxide.

Three cell seeding groups were included: a mono-culture of either activated monocytes or fibroblasts and a co-culture consisting of 90% fibroblasts and 10% activated monocytes. The total number of cells was kept consistent at 100,000 cells per 1 mL collagen construct. After allowing the cell seeded collagen to gel for 60 minutes in a humidified incubator, 1 mL of media comprised of 1X RPMI media and LPS (100 ng/mL) was pipetted into appropriate culture.

In the experiments containing PLGA, the PLGA (2.5 mg/mL) was weighed out and suspended within the collagen solution prior to gelation. The cell culture systems were then incubated in a 37°C humidified incubator with 5% CO_2. For cytokine quantification, supernate from each well was collected (4 hours, 24 hours, 96 hours, 7 days, and 10 days) and centrifuged at 1000 g for 2 minutes at each time point and 500 µL was frozen in -80°C. The media was replaced after each collection and the plate was re-incubated.

Cytokine Quantification

The cell supernates from the 3D collagen gels were loaded into human inflammatory 5-plex magnetic bead kits (Life Technologies, Carlsbad, CA) according to the manufacturer's recommended protocol and analysed on a MagPix (Luminex Corp., Austin, TX). Quantified multiplex protein experiments of human IL-1β, IL-6, IL-8, GM-CSF, and TNF-α were analyzed with a logistics 5P curve fit with seven standards. All the protein experiments are reported in pg/mL.

3.3 Results

The 3D system is composed of activated human monocytes and fibroblasts, key cell types involved in soft tissue inflammation. To confirm monocyte activation, LPS dose and media conditions for these cells was measured in two-dimensional culture using optical microscopy and ImageJ software. Different dosages of LPS were used to elucidate the morphology change

that occurs through this activation. As the dose of LPS increases, the size of the activated monocytes increases (Fig. 3-1a). The unactivated monocytes (Fig. 3-1b) were average size of 12.2 μm (± 2) and the activated cells (Fig. 3-1c) were average size 16.2 μm (± 3) at 0.1 μg/mL LPS and 16.5 μm (± 4) at 1 μg/mL LPS after four hours of incubation (Fig. 3-1). Activated monocytes, treated with 0.1 μg/mL LPS were used in the 3D collagen gel experiments since they are similar to 1μg/mL.

Cell morphology of human monocytes and fibroblasts in 3D culture was observed under phase contrast (Fig. 3-2). Qualitatively, the mono-culture of monocytes remain as individual, spherical cells as they proliferated over the first few days (Fig. 3-2a, 3-2d), whereas the fibroblasts morphology in 3D collagen is stretched with spindle-like extensions reaching out and attaching at various points throughout the gel (Fig. 3-2b, 3-2e). After four days, the co-culture has a distinct effect on the morphology of the monocytes as compared to the mono-culture (Fig. 3-2f, 3-2d respectively), the activated monocytes begin aggregating into colonies within the co-culture. However, the fibroblasts remain spindle-like and dispersed in the co-culture similar to the mono-culture of fibroblasts (Fig. 3-2e - 3-2f).

The inflammatory cytokine protein expression from mono-cultures and co-culture was quantified by a MagPix multiplex magnetic bead system for human IL-1β, IL-6, IL-8, GM-CSF, and TNF-α. There were significantly elevated levels of all five inflammatory cytokines in the co-cultures as compared to the mono-cultures alone (Fig. 3-3a-e). For example, the total GM-CSF expression over ten days is significantly elevated ($p<0.001$) in the co-culture of fibroblasts and activated monocytes versus the mono-cultures alone (Fig. 3-3a). Mono-cultures of fibroblasts expressed 188 pg (± 13) GM-CSF and mono-cultures of activated monocytes expressed levels below the detectable limit; however, co-cultures of activated monocytes and fibroblasts expressed 399 pg (± 9) GM-CSF.

To evaluate the ability of this 3D co-culture system to respond to common biomaterials, PLGA was chosen due to its popularity in research and well documented interaction with human tissues. PLGA microparticles were fabricated by a microemulsion technique (Fig. 3-4a), and their pH changes during degradation were studied in water, 1X RPMI media, and in 3D collagen gel. As expected, the pH decreased (Fig.3- 4b) due to the release of lactic and glycolic acid during hydrolysis (Fig. 3-4c). Although the pH change in buffer containing RPMI and 3D collagen gel did not decrease as much over the ten days (7.7 to 7.1 and 7.5 to 6.9, respectively) as that in water alone (6.8 to 3.3), these magnitudes of pH changes are significant (Fig. 3-4b).

When PLGA microparticles were suspended within cell-seeded 3D collagen gel, elevated levels of IL-1β (159 pg ±8), IL-6 (54305 pg ±3956), GM-CSF (607 pg ±29), and TNF-α (89 pg ±4) were produced when compared to the co-cultures without PLGA (139 pg ±8, 27375 pg ±856, 399 pg ±8, 79 pg ±1, respectively) (Fig. 3-5a). It should be noted that human monocytes alone did not respond to PLGA particles, while monocultures of human fibroblasts release significant levels of IL- 1β (81 pg ±8 with PLGA, 58 pg ±5 without PLGA, $p<0.05$) and IL-6 (10,553 pg ±615 with PLGA, 7,311 pg ±388 without PLGA, $p<0.05$) in response to the PLGA (Fig. 3-6a). Most importantly, when PLGA is exposed to co-culture of fibroblasts and monocytes, there is significantly higher expression of the proteins of all five cytokines tested in the co-culture compared to the fibroblast mono-culture alone ($p<0.001$) (Fig. 3-6).

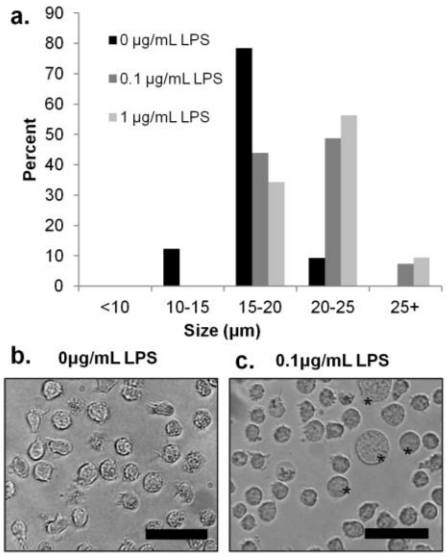

Figure 3-1. Monocyte Pre-Activation with LPS **a.** Monocyte size change with lipopolysaccharide (LPS) concentration. **b.** Monocytes with no activation (0 µg/mL LPS) after 4 hours of incubation. **c.** Monocytes following 4 hours of activation with 0.1 µg/mL LPS. ***** denotes examples of monocytes that have larger diameters. Scale Bar = 50µm

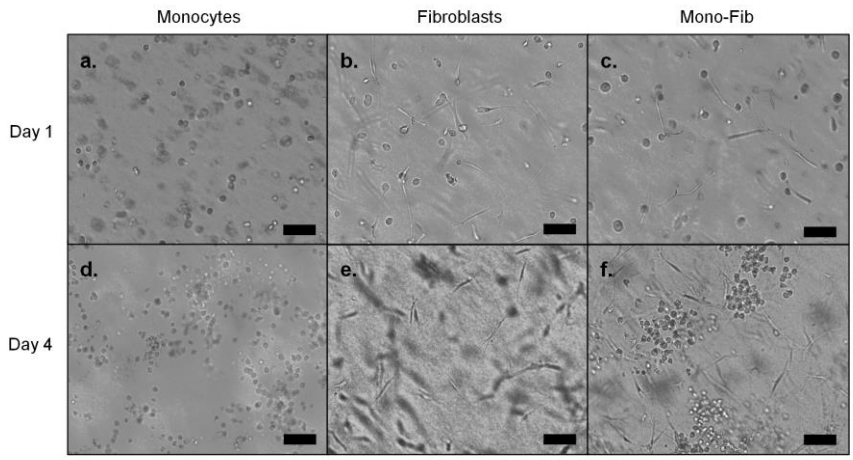

Figure 3-2. Cell morphology in 3D culture system **a-c.** Cells suspended in 3D collagen at Day 1 after initial cell seeding. **d. e.** Day 4 mono-cultures of monocytes and fibroblasts. **f.** Co-culture of monocytes and fibroblasts in the 3D culture at day 4. Images are representative of triplicate experiments (n=3). Scale bar = 100μm.

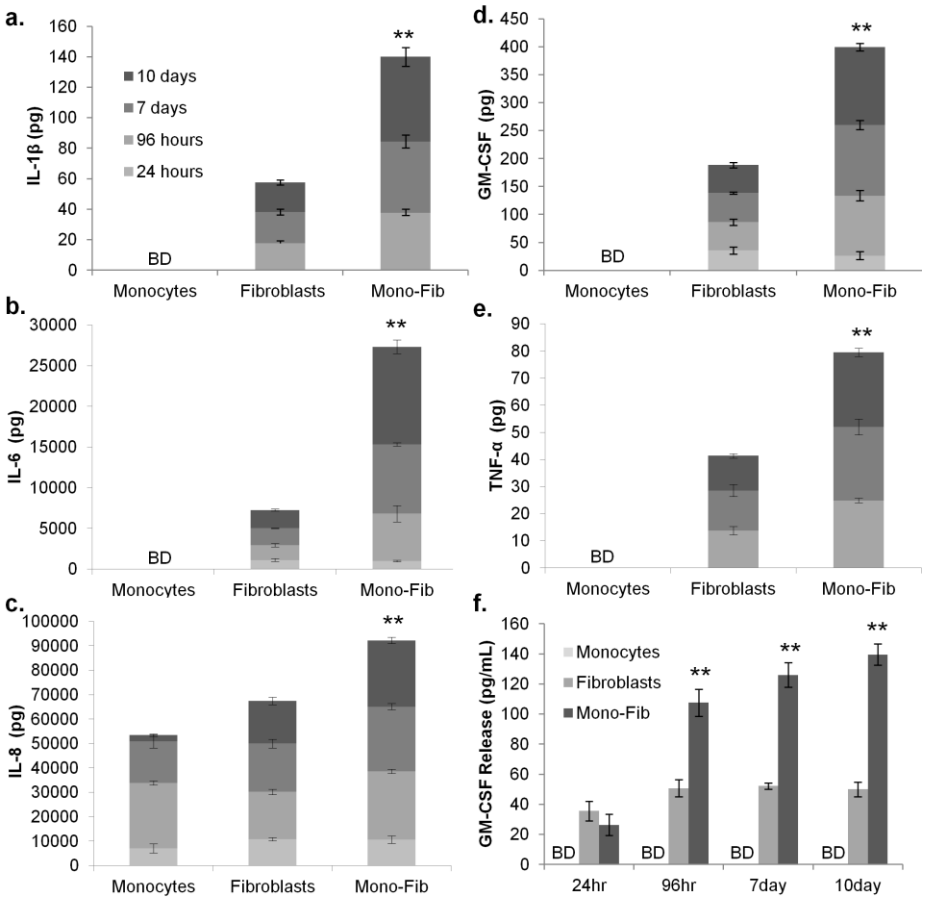

Figure 3-3. 3D Co-culture of cells enhances cytokine release. Release of Inflammatory Cytokines from mono-cultures of activated monocytes or fibroblasts compared to a co-culture of activated monocytes and fibroblasts. Cell supernate protein expression measured on a MagPix instrument. Total Cytokine release over 10 days (pg) **a.** IL-1β, **b.** IL-6, **c.** IL-8. **d.** GM-CSF and **e.** TNF-α. **f.** GM-CSF release profile over time (pg/mL). BD, below detectable limit. ****** denotes a significance of $p<0.001$ for the Mono-Fib co-culture compared to both mono-cultures of monocytes (if applicable) and fibroblasts alone.

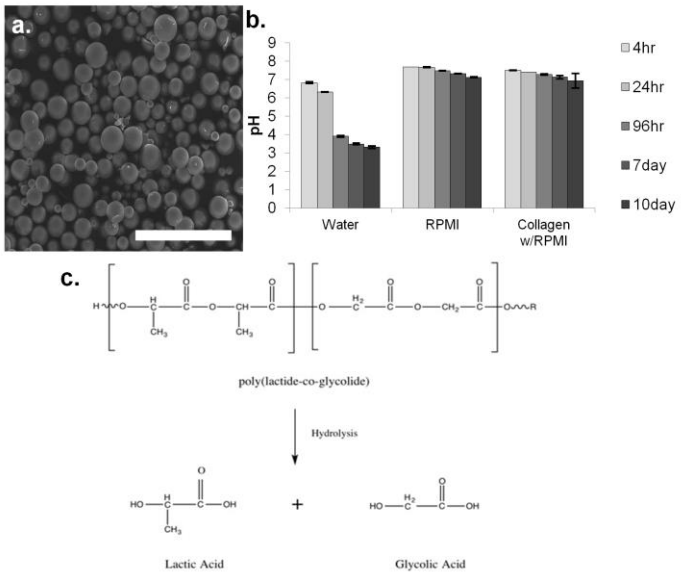

Figure 3-4. PLGA particles and degradation of PLGA **a.** SEM image of the PLGA particles which were then embedded in the 3D collagen model for the co-culture experiments. Scale Bar = 300 µm **b.** A profile of the pH change of PLGA particles in tap water, 1x RPMI media, and suspended in collagen with 1x RPMI media over the collagen construct. **c.** Schematic of the PLGA degradation by hydrolysis.

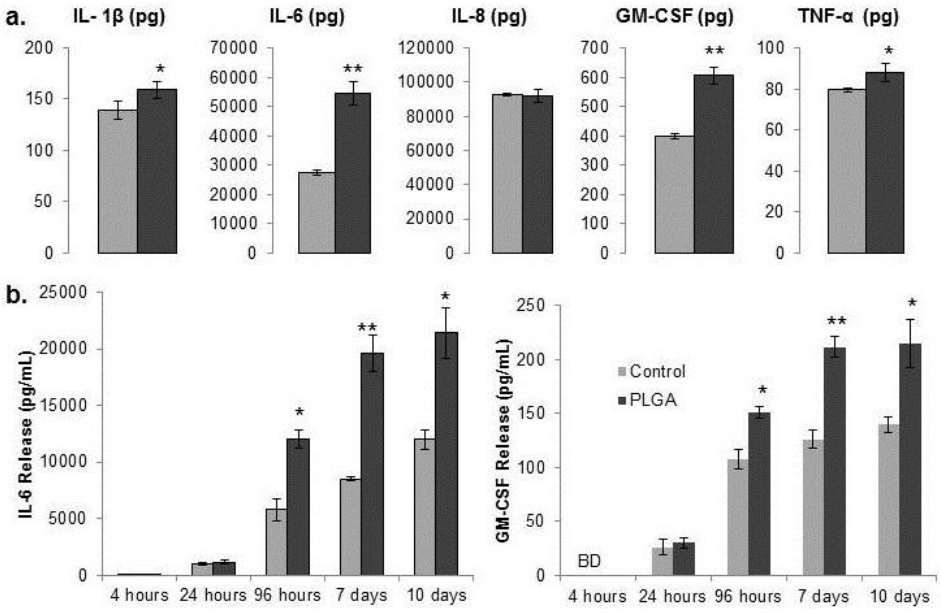

Figure 3-5. PLGA stimulates inflammatory cytokine release in 3D co-culture. **a.** Total inflammatory cytokine release from activated monocyte-fibroblast co-culture experiments over a ten day period with and without PLGA stimulation. **b.** IL-6 and GM-CSF release profiles over time from the 3D in vitro co-culture experiments. Cell supernate protein expression measured on a MagPix instrument. ***** denotes significance with $p<0.05$ and ****** denotes significance with $p<0.001$ when PLGA was added to the co-culture experiments.

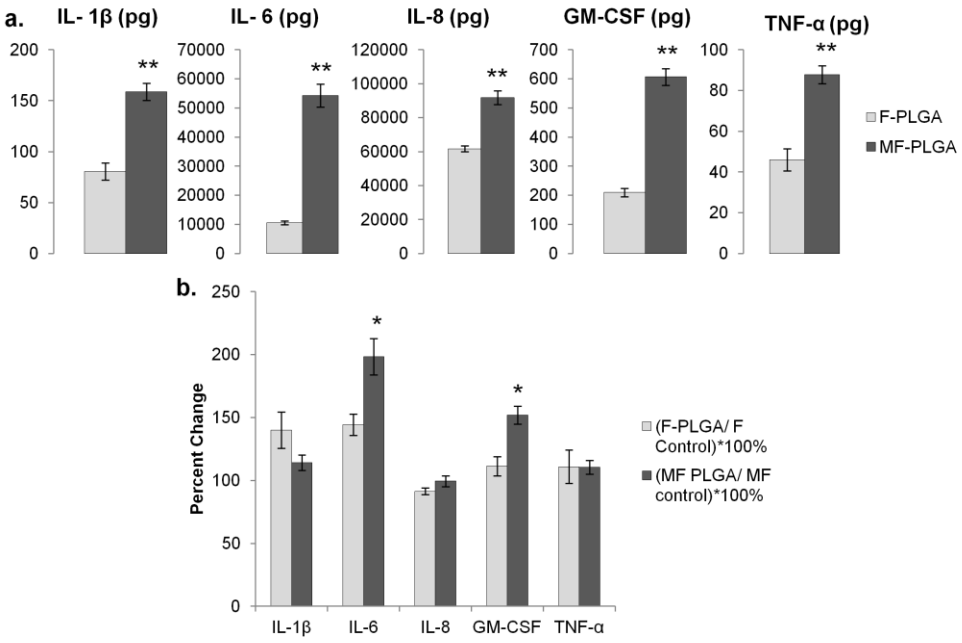

Figure 3-6. PLGA stimulates increased inflammatory cytokine release in 3D co-culture. **a.** Total inflammatory cytokine release from fibroblast and activated monocyte-fibroblast co-culture experiments over a ten day period with PLGA stimulation. Cell supernate protein expression measured on a MagPix instrument. **b.** Percent change of each cytokine due to the addition of PLGA. Percent change = (pg released with stimulation of PLGA/ pg released from respective 3D cell culture)*100. ***** denotes significance with $p<0.05$ ****** denotes significance with $p<0.001$ in the mono-culture vs. the co-culture.

Reference	Culture and Cell Type	Treatment	Findings
mRNA only			
[29]	2D Rat Peritoneal Macrophages	LPS 1.0ug/mL Polymer: 1 g/5 mL of medium	no response to PLGA from unstimulated macrophages IL-1β and TNF-α increase with exposure to PLGA of LPS-stimulated macrophages
[30]	2D HL-60 or NIH/3T3	PLGA 75:25 with or w/o Demineralized bone particles (DBP)	IL-1β and TNF-α expression in HL-60 is high in response to PLGA as compared to PLGA with DBP *in vivo* - more neutrophils and FBGCs in PLGA than in PLGA with DBPs
[31]	2D HL-60 or NIH/3T3	PLGA 75:25 with or w/o 2-methacryloyloxyethyl phosphorylcholine	IL-1β expressed from HL-60 cells adhered on PLGA was about ten times more than that on the PLGA/PMEH membrane
[35]	2D transwell human gingival fibroblasts and u937 monocytes or human blood derived monocytes	LPS - 100ng/mL	MMP-1 and IL-6 are upregulated in co-culture compared to mono-culture IL-6 is released from fibroblasts and acts on u937 to further release more IL-6
[36]	2D HL-60	PMA 50nM and LPS 10ug/mL	IL-1β levels change with contact angle (hydrophilicity) of material surfaces
Protein Quantification			
[16]	3D collagen HFL-1 fibroblasts and human blood derived monocytes	exogenous PGE2 and IL-1β and TNF-α	increase in IL-1β and TNF-α in co-culture (no expression in mono-cultures)
[24]	2D u937 monocytes	LPS-100ng/mL	IL-8 is produced from u937s
[26]	2D human fibroblasts and blood derived monocytes	exogenous GM-CSF IL-4 or IL-6 to monocultures or analyze co-cultures	IL-6 produced from fibroblasts encouraged monocyte differentiation to macrophages production of the differentiating factor(s) required monocyte and fibroblast contact, as the supernatants of fibroblasts (stimulated with GM-CSF and IL-4) did not promote macrophage differentiation
[28]	2D J774 murine macrophage-like cells	PLGA 50:50 78kDa LPS 0.5ug/mL	IL-1β and TNF-α both increase with exposure to PLGA microparticles (not nano-particles)
[34]	2D transwell NHDF fibroblasts and human blood derived monocytes	PEG siPN or transwell PC membrane	GMCSF and MMP-2 are increased in co-culture as compared to mono-culture
[37]	2D primary human ginigival fibroblasts	LPS - 1ug/mL	IL-6 expression is high in LPS treated fibroblasts, expression can be lowered or inhibited by Vitamin K compounds
[38]	2D u937 monocytes	GM-CSF (10ng/mL) + IL-6 (0-20ng/mL) LPS added (0-1000ng/mL)	no TNF production from u937s alone or with just LPS stimulation - u937s are activated with GM-CSF (similar reaction to PMA), IL-6 has an inhibitory effect of TNF production in u937s
[41]	2D human derived monocytes	LPS- varied concentrations	LPS stimulates TNF expression
Protein Quantification and mRNA			
[18]	3D gelatin and alginate - primary mouse fibroblasts and macrophages		All the inflammatory cytokines detected in the macrophages/fibroblasts co-culture were significantly greater ($p<0.05$) than those of the macrophages monoculture. IL-6 was downregulated in co-culture compared to fibroblast mono-culture.
[27]	2D primary human fibroblasts	IL-1α or Conditioned media from NHK	Elevated IL-6 and IL-8 levels in fibroblast cultures with keratinocyte conditioned media or IL-1α introduction
[39]	2D human blood derived monocytes	LPS - 10ng/mL	LPS stimulates TNF-α and IL-6 production
[42]	2D transwell THP-1 monocyte and A549 epithelial cells	mercaptoethanol	mRNA levels: IL-1, IL-6, IL-8 increased over the experiment period; Protein analysis: IL-8 upregulated early on; IL-1 and IL-6 upregulated at later time points; GM-CSF and IL-6 have no protein expression until 24 hours and only in the co-culture
[44]	2D human blood derived monocytes	LPS - 1ug/mL	TLR-4 surface expression upregulated in LPS treated monocytes; IL-1β and TNF-α increase with LPS

Table 3-1. Inflammatory response quantification methods from related 2D and 3D cell culture types.

3.4 Discussion

The 3D human soft tissue model comprised of activated human monocytes and human fibroblasts in a collagen gel construct. The utility of this model is evident by the fact that an ECM protein hydrogel is used as the 3D construct instead of a synthetic or non-ECM hydrogel. Additionally, human cell lines are utilized in a co-culture as opposed to rodent cell lines. To date there has not been a representative human cell soft tissue *in vitro* model to study host-material interaction. Zeng et al. analyzed inflammatory cytokine release in a non-ECM alginate hydrogel co-culture of mouse fibroblasts and monocytes(18). This previous publication, along with others (Table 3-1), led to our motivation to develop an ECM protein based scaffold with human cells and quantify inflammatory cytokine release profiles in our research.

The cell-cell interaction and subsequent response are seen when the cell types are cultured together in the three dimensional soft tissue model. Specifically, the optical images show a difference in morphology and overall organization (Fig. 3-2). In the single cell culture of activated monocytes in 3D, there is no morphology change. However, when the activated monocytes are combined with the fibroblasts, there is colony formation amongst the monocytes early on in the experiments (Fig.3- 2f). This colony formation mimics physiological behavior of monocytes, perhaps due to the interaction between the fibroblasts and monocytes which could cause the release of colony stimulating factors that promote the grouped orientation.

GM-CSF is a pro-inflammatory protein that is released by fibroblasts and macrophages(19) and is a cytokine that induces the transition of monocytes to macrophages(20). Additionally, IL-6 is required as a co-factor to induce colony formation of human bone marrow progenitor cells(21). Together, IL-6 and GM-CSF may act additively or synergistically on the observed cell aggregation within the 3D co-culture (Fig. 3-3b and 3-3d). Since the U937 cell line is a monocytic cell-type, there is no GM-CSF expression when they are in culture alone (Fig. 3-3d and 3-3f). However, when cultured with fibroblasts, there is elevated

levels of GM-CSF and IL-6 which indicate the activation and differentiation of the monocytic cell line through the co-culture interaction with fibroblasts (Fig. 3-3f).

Other cytokines associated with the acute phase of wound repair include the family of interleukins. IL-1β induces inflammation by stimulating production of IL-6 and IL-8. While monocytes themselves do not secrete IL-6 until they are activated to macrophages, they do secrete IL-8(22–24). This could explain the lack of interleukin secretion from the monocytes alone, however when they are cultured with the fibroblasts, they become activated and there are higher levels of interleukins 1, 6, and 8 (Fig. 3-3).

Monocytes and macrophages are not the only cells that secrete and react to cytokine factors. Fibroblasts secrete some IL-6 when in culture alone (7311 pg ±388), however when cultured with the activated monocytes, the protein expression is much higher over a ten day period (10,553 pg ±615) ($p<0.001$) (Fig. 3-3). IL-6 has been shown to be expressed by a variety of cells, including endothelial cells, keratinocytes, and fibroblasts, as well as macrophages(25). Our data corroborates this with the expression of interleukins from the mono-culture of fibroblasts (Fig. 3-3). Upon IL-6 release by neighboring fibroblasts, monocytes undergo a self-regulating mechanism that further induces their differentiation into macrophages(26). Fibroblasts also secrete IL-1β and IL-8 which then act upon monocytes and macrophages to increase inflammation, through activation of macrophages and recruitment of monocytes(27). Levels of IL-1β, IL-6, IL-8, GM-CSF, and TNF-α are all elevated in the monocyte-fibroblast co-culture as compared to the mono-cultures alone over the ten day incubation period (Fig. 3-3). This finding is in contrast to the analysis of similar rodent cell types. Zeng et al. found down-regulated cytokines (IL-6 and GM-CSF) in a co-culture of murine cells compared to a mono-culture of fibroblasts(18). Our human cell lines exhibited an increase in not only IL-6 and GM-CSF, but also IL-1β, IL-8, and TNF-α as well when in co-culture. However, both the murine cell types and the human cell lines had an increase in cytokine expression in the co-culture

compared to the monoculture of monocytes(18). Our 3D *in vitro* system showed the importance of having a human cell co-culture which is physiologically relevant.

The elevated expression of inflammatory cytokines shows the beginning of the inflammatory signal from the two cell types as they have cell-cell and cell-matrix interactions. The cytokine release suggests the cells are starting to mature and interact with one another. Models such as the one presented here are closely related to the responses which are expected *in vivo*, however there is a higher level of control over the various parameters of the experiment *in vitro*.

To test this soft tissue model as a way to quantify the inflammatory properties of the host-biomaterial interactions, PLGA particles (Fig. 3-4) were introduced to the 3D culture system and the cytokine expression was analyzed. PLGA is known to induce short term inflammation in humans, and has been shown to stimulate an increase in tumor necrosis factor-alpha (TNF-α) and interleukin-1 beta (IL-1β) release from macrophages (Table 3-1)(28–30). The exposure of the co-culture to PLGA further stimulates it and yields elevated expression of inflammatory cytokines IL-1β, IL-6, GM-CSF, and TNF-α (Fig. 3-5a). This is expected based on previous two dimensional findings of macrophages and fibroblasts cultured separately with elevated mRNA levels of IL-1β and TNF-α in response to PLGA (Table 3-1)(28–31). Example data of each time point taken can be seen in figure 5b which shows the release of IL-6 and GM-CSF over time from the co-cultures. The significant elevation of the inflammatory cytokines is evidence that the activated monocytes and fibroblasts are not only interacting with one another in the co-culture (Fig. 3-3), but they are also reacting to the exposure of PLGA (Fig. 3-5).

When the PLGA reaction was analyzed further, the values of the fibroblasts stimulated with PLGA and the co-culture stimulated with PLGA are normalized to their respective cell types without PLGA. The percent change over the ten day period is similar for IL-1β, IL-8, and TNF-α indicating that most of the reaction to the PLGA is from the fibroblasts within the co-culture (Fig.

3-6b). However, the percent change for IL-6 and GM-CSF due to PLGA are significantly elevated ($p<0.05$) in the co-culture compared to the mono-culture of fibroblasts. This suggests that the activated monocytes are either enhancing the fibroblasts' production of these factors, or the monocytes are secreting the factors themselves.

The significant elevation of inflammatory cytokines over the ten day period is important to understand the expected interaction *in vivo*. It has been seen in a PLGA micro-particle plasmid delivery system model that PLGA recruits macrophages and foreign body giant cells to the region upon *in vivo* implantation(30,32). The *in vitro* model introduced in this work aims to bring out the protein expression result from this inflammatory response. It is well understood that PLGA can cause inflammation(33), however the specific cytokine protein production has not been analyzed in three dimensional human cell co-culture until this study. The three-dimensional co-culture data corroborates to pre-existing literature comparing two-dimensional studies of IL-1β and TNF-α to *in vivo* findings of increased inflammation due to PLGA(28–30,34). This suggests that our *in vitro* system can recapitulate the *in vivo* setting (Table 3-1). Ultimately, the goal of developing a model such as the one in this research is to facilitate the investigation of the effects that drugs, cofactors, or biomaterials have on the inflammatory response by having a simple, reproducible, physiologically relevant 3D *in vitro* model similar to that of human tissues.

This work builds on the importance of analyzing cell studies in a more natural 3D microenvironment versus a 2D cell culture. The elevated cytokine expression in the co-culture further shows the importance of having physiologically similar models to test biomaterials in. There is great importance in studying cells in a 3D microenvironment as well as the subsequent analysis of biomaterials in this setting. This is a growing area of interest due to the importance of understanding host-biomaterial interactions before incorporation of the material into a commercial product. The *in vitro* soft tissue model that has been developed can be tailored to

more closely mimic other tissues in the body and their relevant responses to aid in the screening of biomaterials and provide additional information to proceed with animal studies.

3.5 References

1. DiPietro LA. Wound Healing: The Role of the Macrophage and Other Immune Cells. Shock. 1995 Jun 22;Vol. 4(No. 4):pp 233–240.
2. Gorbet MB, Sefton MV. Biomaterial-associated thrombosis: roles of coagulation factors, complement, platelets and leukocytes. Biomaterials. 2004 Nov;25(26):5681–703.
3. Anderson JM, Rodriguez A, Chang DT. FOREIGN BODY REACTION TO BIOMATERIALS. Semin Immunol. 2008 Apr;20(2):86–100.
4. Festing MFW, Altman, Douglas G. Guidelines for the Design and Statistical Analysis of Experiments Using Laboratory Animals. Inst Lab Anim Res. 2002;43(4):244–58.
5. Collins LM, Dziak JJ, Li R. Design of Experiments with Multiple Independent Variables: A Resource Management Perspective on Complete and Reduced Factorial Designs. Psychol Methods. 2009 Sep;14(3):202–24.
6. Cukierman E, Pankov R, Stevens DR, Yamada KM. Taking Cell-Matrix Adhesions to the Third Dimension. Science. 2001 Nov 23;294(5547):1708–12.
7. Yamada KM, Cukierman E. Modeling Tissue Morphogenesis and Cancer in 3D. Cell. 2007 Aug 24;130(4):601–10.
8. Doyle AD, Petrie RJ, Kutys ML, Yamada KM. Dimensions in cell migration. Curr Opin Cell Biol. 2013;25:1–8.
9. Li N, Wang D, Sui Z, Qi X, Ji L, Wang X, et al. Development of an Improved Three-Dimensional *In Vitro* Intestinal Mucosa Model for Drug Absorption Evaluation. Tissue Eng Part C Methods. 2013 Apr 21;19(9):708–19.

10. Thomas RJ, Bhandari R, Barrett DA, Bennett AJ, Fry JR, Powe D, et al. The Effect of Three-Dimensional Co-Culture of Hepatocytes and Hepatic Stellate Cells on Key Hepatocyte Functions in vitro. Cells Tissues Organs. 2005;181(2):67–79.
11. Ho WJ, Pham EA, Kim JW, Ng CW, Kim JH, Kamei DT, et al. Incorporation of multicellular spheroids into 3-D polymeric scaffolds provides an improved tumor model for screening anticancer drugs. Cancer Sci. 2010;101(12):2637–43.
12. Kim JW, Ho WJ, Wu BM. The Role of the 3D Environment in Hypoxia-induced Drug and Apoptosis Resistance. Anticancer Res. 2011 Oct 1;31(10):3237–45.
13. Takahashi M, Kitagawa S, Masuyama J-I, Ikeda U, Kasahara T, Takahashi Y-I, et al. Human Monocyte–Endothelial Cell Interaction Induces Synthesis of Granulocyte-Macrophage Colony-Stimulating Factor. Circulation. 1996 Mar 15;93(6):1185–93.
14. Randolph GJ, Beaulieu S, Lebecque S, Steinman RM, Muller WA. Differentiation of Monocytes into Dendritic Cells in a Model of Transendothelial Trafficking. Science. 1998 Oct 16;282(5388):480–3.
15. Dutta RC, Dutta AK. Cell-interactive 3D-scaffold; advances and applications. Biotechnol Adv. 2009 Jul;27(4):334–9.
16. Zhu Y, Sköld CM, Liu X, Wang H, Kohyama T, Wen F-Q, et al. Fibroblasts and monocyte macrophages contract and degrade three-dimensional collagen gels in extended co-culture. Respir Res. 2001 Sep 4;2(5):295.
17. Dikovsky D, Bianco-Peled H, Seliktar D. The effect of structural alterations of PEG-fibrinogen hydrogel scaffolds on 3-D cellular morphology and cellular migration. Biomaterials. 2006 Mar;27(8):1496–506.
18. Zeng Q, Chen W. The functional behavior of a macrophage/fibroblast co-culture model derived from normal and diabetic mice with a marine gelatin–oxidized alginate hydrogel. Biomaterials. 2010 Aug;31(22):5772–81.

19. Shi Y, Liu CH, Roberts AI, Das J, Xu G, Ren G, et al. Granulocyte-macrophage colony-stimulating factor (GM-CSF) and T-cell responses: what we do and don't know. Cell Res. 2006;16(2):126–33.
20. Hamilton JA. GM-CSF in inflammation and autoimmunity. Trends Immunol. 2002 Aug 1;23(8):403–8.
21. Jansen JH, Kluin-Nelemans JC, Damme JV, Wientjens GJ, Willemze R, Fibbe WE. Interleukin 6 is a permissive factor for monocytic colony formation by human hematopoietic progenitor cells. J Exp Med. 1992 Apr 1;175(4):1151–4.
22. Guo Y, Lip GYH, Apostolakis S. Inflammation in Atrial Fibrillation. J Am Coll Cardiol. 2012 Dec 4;60(22):2263–70.
23. Neumann F-J, Ott I, Marx N, Luther T, Kenngott S, Gawaz M, et al. Effect of Human Recombinant Interleukin-6 and Interleukin-8 on Monocyte Procoagulant Activity. Arterioscler Thromb Vasc Biol. 1997 Dec 1;17(12):3399–405.
24. Labéta MO, Vidal K, Nores JE, Arias M, Vita N, Morgan BP, et al. Innate recognition of bacteria in human milk is mediated by a milk-derived highly expressed pattern recognition receptor, soluble CD14. J Exp Med. 2000 May 15;191(10):1807–12.
25. Van Snick J. Interleukin-6: An Overview. Annu Rev Immunol. 1990;8(1):253–78.
26. Chomarat P, Banchereau J, Davoust J, Karolina Palucka A. IL-6 switches the differentiation of monocytes from dendritic cells to macrophages. Nat Immunol. 2000 Dec;1(6):510–4.
27. Boxman ILA, Ruwhof C, Boerman OC, Löwik CWGM, Ponec M. Role of fibroblasts in the regulation of proinflammatory interleukin IL-1, IL-6 and IL-8 levels induced by keratinocyte-derived IL-1. Arch Dermatol Res. 1996 Jun 1;288(7):391–8.

28. Nicolete R, Santos DF dos, Faccioli LH. The uptake of PLGA micro or nanoparticles by macrophages provokes distinct in vitro inflammatory response. Int Immunopharmacol. 2011 Oct;11(10):1557–63.
29. Ding T, Sun J, Zhang P. Immune evaluation of biomaterials in TNF-alpha and IL-1beta at mRNA level. J Mater Sci Mater Med. 2007 Nov;18(11):2233–6.
30. Yoon SJ, Kim SH, Ha HJ, Ko YK, So JW, Kim MS, et al. Reduction of inflammatory reaction of poly(d,l-lactic-co-glycolic Acid) using demineralized bone particles. Tissue Eng Part A. 2008 Apr;14(4):539–47.
31. Iwasaki Y, Sawada S, Ishihara K, Khang G, Lee HB. Reduction of surface-induced inflammatory reaction on PLGA/MPC polymer blend. Biomaterials. 2002 Sep;23(18):3897–903.
32. Soderquist RG, Sloane EM, Loram LC, Harrison JA, Dengler EC, Johnson SM, et al. Release of Plasmid DNA-Encoding IL-10 from PLGA Microparticles Facilitates Long-Term Reversal of Neuropathic Pain Following a Single Intrathecal Administration. Pharm Res. 2010 May;27(5):841–54.
33. Anderson JM, Shive MS. Biodegradation and biocompatibility of PLA and PLGA microspheres. Adv Drug Deliv Rev. 2012 Dec;64, Supplement:72–82.
34. Chung AS, Kao WJ. Fibroblasts regulate monocyte response to ECM-derived matrix: The effects on monocyte adhesion and the production of inflammatory, matrix remodeling, and growth factor proteins. J Biomed Mater Res A. 2009;89A(4):841–53.

CHAPTER FOUR

IN VIVO ANALYSIS OF MACROPOROUS PCL MICROPARTICLES WITH A BIOACTIVE PLGA COATING

4.1 Introduction

Many types of polymers have been FDA approved for various uses; from large size implants to suture materials (1,2). Polymers have favorable mechanical properties, application versatility, and relatively low reactivity within the body (3–5) which makes them very appealing for many biomedical applications. Even though there are many benefits to implanting polymers, there are also drawbacks, including low tissue integration. In order to maintain the success of an implant, it must integrate with native tissue, however bulk polymer scaffolds don't integrate well due to lack of cell infiltration. Pores can be created during most polymer fabrication methods as a way of increasing cell infiltration into the scaffolds (6,7). However, diffusion limited cell survival is considered to be <1mm into the scaffold (or $\phi<1$), therefore, cell infiltration is only sustainable if there is vasculature to bring nutrients and remove waste from the area (8–10). There are two strategies to achieve nutrient and oxygen diffusion through the scaffold: increase vascularization within a scaffold or to miniaturize implant size. Increasing vascularization is difficult to control because growth factors and signals such as vascular endothelial growth factor (VEG-F) are needed as well as properly interconnected pores to allow for angiogenesis within a scaffold structure (11,12). This limitation has motivated the need to miniaturize scaffold implants to allow for sufficient cell survival in and around an implant.

One benefit to smaller scale implants is that the delivery method can more easily be via needle injection, rather than an open wound implantation. Injectable polymers have historically been used as filler or bulking agents for dermal augmentation or other soft tissue bulking such as that of the periurethral region or the esophageal sphincter (3,13,14). Dermal injectables vary from naturally occurring materials such as collagen, to synthetic polymeric materials with

varying geometries, such as silicon micro-droplets or microparticles. Unfortunately, most naturally occurring dermal soft tissue fillers are liquid or hydrogel based and degrade in the body within 3-9 months (15,16) which does not allow for an extended aesthetic effect. Semi-permanent and permanent soft tissue fillers have been created to last for longer periods of time, however, they tend to have adverse reactions over time (17,18). For example, the injectables that contain either polymethyl methacrylate (PMMA) or poly-lactic acid (PLA) microspheres (size range: 30-60 μm) can last for up to two years with PLA microspheres and even longer in the case of PMMA microspheres. The smooth solid surface of the microsphere makes it so that they must be treated like a foreign body and fibrous encapsulated to augment the area for an extended period of time (14). However, the fibrous capsule can grow too thick and cause nodules to form at the skin's surface due to a chronic immune response. With ArteColl (hyaluronic acid with PMMA microspheres), foreign body response is known to last over ten years (19). The undesirable aesthetic effect of skin nodules makes the semi-permanent and permanent dermal fillers not as appealing (14,18). Additionally, it has been seen that smooth surface implants are more likely to have migration of wear particles, whereas a porous implant is integrated into existing tissue (20). Therefore, these weaknesses point to the need for a long term injectable implant that does not cause a chronic foreign body response and results in integration and augmentation that can be maintained for years.

Previously, macroporous poly ε-caprolactone (PCL) microparticles have been fabricated with varying size range (21). PCL is FDA approved in material implants and has an additional advantage that it has been demonstrated to last for years *in vivo* (22–24). PCL is a polymeric material that has been utilized for a variety of biomaterial applications from bone tissue engineering to microparticle drug delivery systems (25–27). The macroporous PCL microparticles (21) have surface porosity and internal interconnectivity of pores. These particles

have the potential to overcome the need for total fibrous encapsulation to maintain their volume augmentation, instead they allow for cell infiltration (21) which can lead to tissue integration.

It has been seen in other facets of research, such as bone tissue regeneration that there is a need for accelerated wound healing in order to integrate and anchor an implant into existing tissue (28). To encourage accelerated tissue deposition and decreased healing time, the macroporous PCL microparticles have been coated in poly(lactic-co-glycolic acid) (PLGA). PLGA has been shown to increase inflammation (29,30) and result in an increase in matrix deposition in a vascular aneurysm model (31). Therefore, in this model, the PLGA coating is used to encourage increased collagen deposition by activating an immune response. This allows for particle integration into native tissue more quickly.

4.2 Materials and Methods

Microparticle fabrication

Macroporous PCL microparticles were fabricated using a double emulsion technique as previously described (21). Briefly, the primary emulsion was prepared by dissolving PCL in dichloromethane overnight and vortexing with an ammonium bicarbonate in water solution. This primary emulsion was poured into a spinning poly vinyl alcohol solution and allowed to magnetically stir for two hours while the solvent to evaporated. Macroporous microparticles were subsequently washed and lyophilized.

Bioactive Coating

PLGA (50:50 Lakeshore Biomaterials) was coated onto the surface of the macroporous PCL microparticles using a pressurized air brush (Master Airbrush, TCP Global) and a 1% PLGA in acetone (Fisher) solution (w/v). The dry PCL particles (average size = 520µm) were sandwiched between two sieves (45µm below and 75µm above) and the PLGA solution was spray coated onto the surface of the microparticles. Subsequently, the particles were analyzed on a scanning electron microscope (SEM) to assess for any changes from the coating process.

Murine Implantation and Harvesting

C57BL/6 mice (age 10-13 weeks) were purchased from Charles River Laboratories, Wilmington, MA. The animals were handled in compliance with the institutional regulations established and approved by the Animal Research Committee at the University of California, Los Angeles. For scaffold implantation, mice were anesthetized with isofluorane and a 1-cm long dorsal midline incision was made to create a subcutaneous pocket. A laser-cut PCL sheet (~200μm) was rolled into a tube and filled with microparticles then inserted in the subcutaneous pocket about a centimeter away from the incision and the skin was sutured with 3-0 Vicryl (Ethicon, Somerville, NJ). One scaffold was implanted in each mouse.

The animals were sacrificed at 1 week, 2 weeks, and 4 weeks post-implantation. The scaffolds, along with adjacent subcutaneous tissue were harvested and fixed promptly in 10% formalin overnight at 4°C.

The fixed samples were paraffin embedded and sectioned into 5μm slices. The deparaffinized sections were stained with hematoxylin and eosin (H&E) and used to verify cell infiltration into the PCL implants.

Immunohistochemistry (IHC)

Deparaffinized sections were stained for either CD68 (monocyte/macrophage cells), CD31 (endothelial cells) or collagen (picrosirius red). Anti-CD68 primary antibody and AlexaFluor 488 secondary antibody (Abcam) were used to fluorescently label inflammatory cells. The slides were imaged under a GFP filter on an Olympus fluorescent microscope and stained sections were compared to no primary controls to ensure proper staining. CD68 labels monocyte and macrophage cells as well as foreign body giant cells within the tissue section. Anti-CD31 primary antibody (Abcam) was followed by a biotinylated secondary antibody (Vector Labs) and horseradish peroxidase streptavidin, then finally a 3,3'-Diaminobenzidine (DAB) chromogen solution was developed for 10 minutes (Vector Labs). Hematoxylin was used as a

counter stain. This staining procedure resulted in CD31+ cells developing a brown exterior membrane color. CD31 labels endothelial cells indicating the lining bloods vessels; it can also weakly label monocytic cells.

Picrosirius Red (Poly sciences) stain was used to image deposited collagen fibers. Using polarized filters on a bright field scope, collagen fibers birefringe and can be identified. Collagen deposition is used to verify tissue integration and extracellular matrix deposition.

IHC Image Quantification

Image quantification was performed on ImageJ software (NIH). The analyze particle function was utilized to obtain a total area stained for the fluorescent CD68 and polarized picrosirius red stained samples and this was expressed as a percent area. The CD31 brightfield images were analyzed for total blood vessel number and distance of the vessels from the surface of the implanted pouch. Statistical significance was determined using the student's t-test and a value of $p<0.05$ was considered significant and a value of $p<0.01$ was considered very significant.

4.3 Results

Cell Infiltration

The H&E images (Fig. 4-1) show that cells get past the implant surface and to the microparticles themselves over time. At one week, there is very little cell infiltration into the scaffolds. However, the images show that with time more cells infiltrate into the implants and occupy the space between the polymer particles. The macroporous PCL particles allow for additional cell infiltration into the bulk of the particles, whereas the non-porous particles have no cells on the interior of the particles. Qualitatively, at week 2 and week 4 macroporous PCL microparticles with PLGA coated onto the surface have the greatest number of cells.

Collagen Deposition

Collagen deposition was analyzed to elucidate healing around the particles within the body (Fig. 4-2). The images show that collagen is deposited only around the surface of the non-porous particles, whereas the porous particles have collagen deposition within the particles themselves, indicating that the cells that infiltrated are depositing their own extracellular matrix. There was a higher amount of collagen deposition over time within each scaffold type (Fig. 4-4a) as compared to the earlier time points. However, the non-porous had the least collagen deposition while the PLGA coated scaffolds had the most. Additionally, statistically significant levels of the collagen deposition was seen at 2 weeks and 4 weeks post-implantation in the porous particles over the non-porous particles ($p= 0.027$ and $p= 0.0012$, respectively). Furthermore, collagen deposition was significantly higher in PLGA coated porous particles over non-coated porous particles at 2 weeks ($p= 6.3E-04$) and 4 weeks ($p= 1.6E-04$) (Fig. 4-4a).

Blood Vessel Infiltration

Vascularization was analyzed using CD31 antibodies to stain for endothelial cells (Fig. 4-3). It was seen in the murine model that the macroporous PCL microparticles had significantly higher number of blood vessels (Fig. 4-4b) at 2 weeks (porous = 17±1.2, non-porous = 8.3±0.77) ($p= 0.038$) and 4 weeks (porous = 38±0.97, non-porous = 12±0.66) ($p= 4.7E-06$) when compared to the non-porous samples. The addition of PLGA causes an enhanced effect on blood vessel formation in that there are a higher average number (2 week = 27±1.6, 4 week = 50±1.2) of blood vessels overall in the samples ($p= 0.042$ and $p= 0.011$, respectively). At the 4 week timepoint, blood vessel infiltration depth into the implant was significantly greater in the porous particles over the non-porous particles (Fig. 4-4c) ($p= 5.3E-07$). Blood vessel infiltration depth was significantly further in PLGA coated samples over non-coated samples at 2 weeks ($p= 8.4E-08$) and 4 weeks ($p= 4.3E-08$) (Fig. 4-4c).

Immune Response

The implanted scaffolds were analyzed for inflammation via CD68 expression (Fig. 4-5). CD68 labels the cell surface of monocytes and macrophages as well as when they join to form foreign body giant cells. From the fluorescent images, it can be seen that there is the most expression in the samples coated in PLGA. After quantification, it was found that CD68 was significantly higher at 2 weeks and 4 weeks post-implantation in the PLGA coated samples compared to the macroporous PCL alone ($p= 7.08E-07$ and $p= 0.0071$) (Fig. 4-6). This indicates that the PLGA is having an inflammatory effect on the implants.

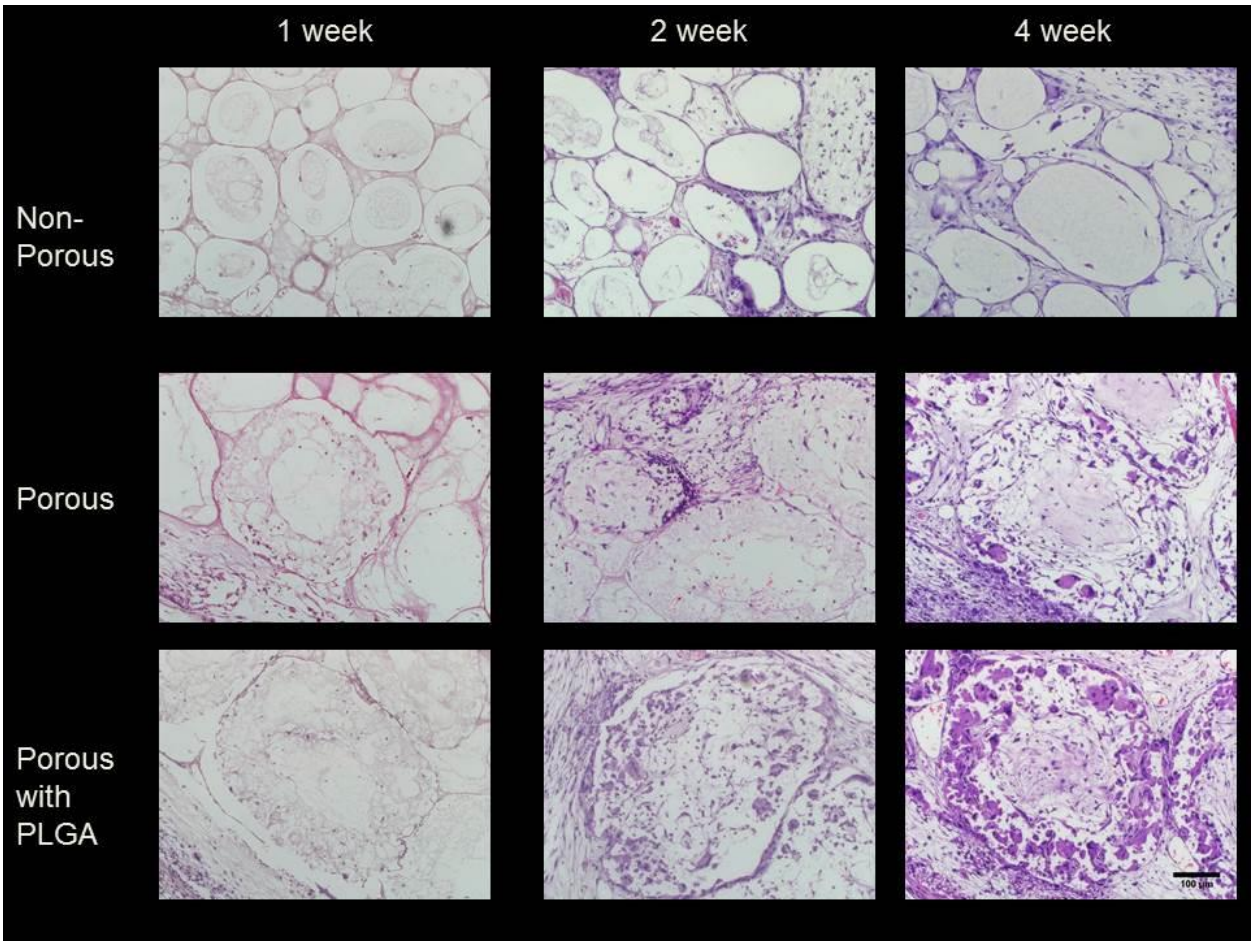

Figure 4-1. Hematoxylin and Eosin staining of explants from the subdermal murine model. Scale bar 100 µm. Magnification 200X.

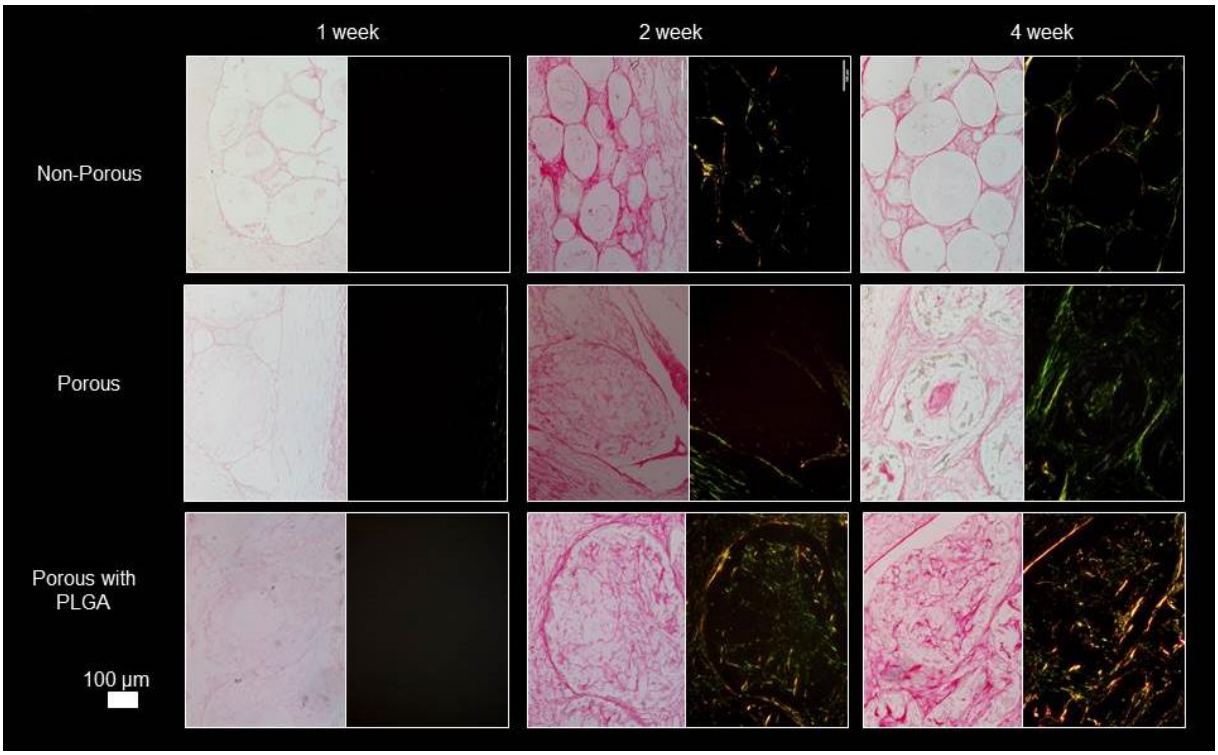

Figure 4-2. Picrosirius Red Staining for collagen deposition. Bright-field images and polarized birefringent images are of the same respective areas. Scale bar = 100µm. Magnification 200X.

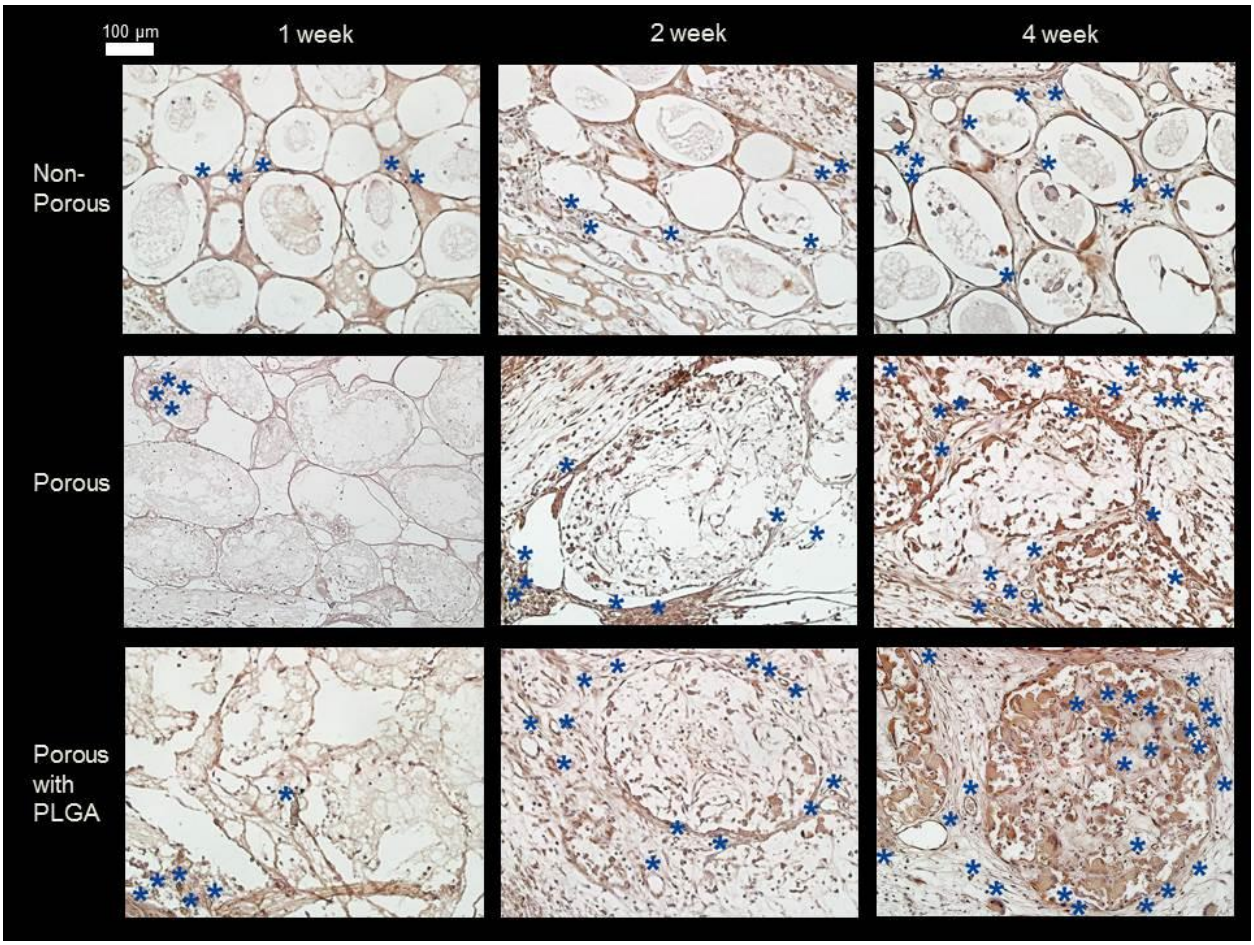

Figure 4-3. CD31 staining of vascularization. ***** denotes location of a blood vessel. Scale Bar = 100µm. Magnification 200X

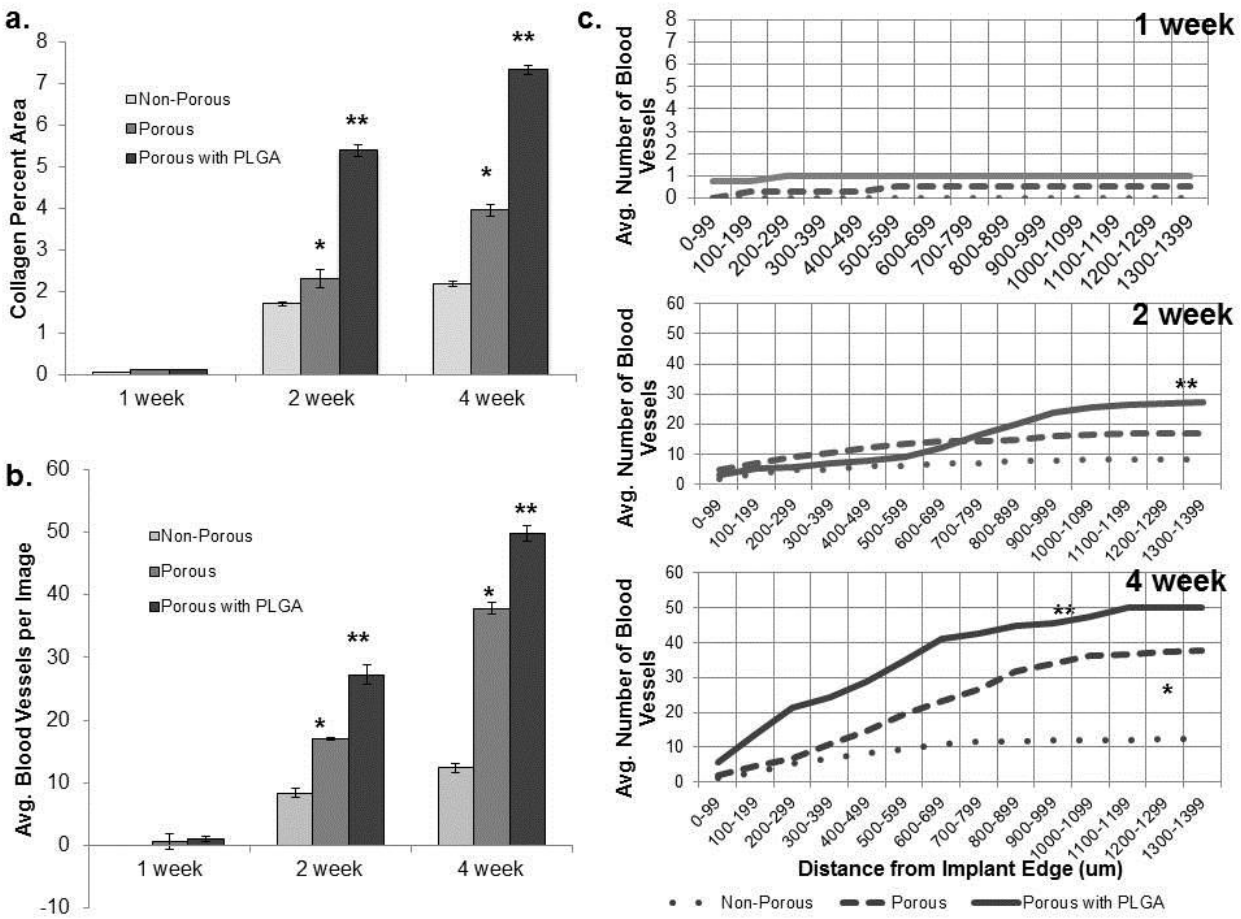

Figure 4-4. Quantification of Immunohistochemical Analysis. **a.** Quantification of picrosirius red staining labeling collagen deposition within the scaffold implants. **b.** Average number of blood vessels per image based on CD31 staining. **c.** Cumulative average distance that blood vessels infiltrate into scaffold. Statistical Analysis performed using student's t-test with $p<0.05$ indicating significance. * denotes statistical significance between porous and non-porous PCL particles. ** denotes statistical significance between PLGA coated and porous PCL particles.

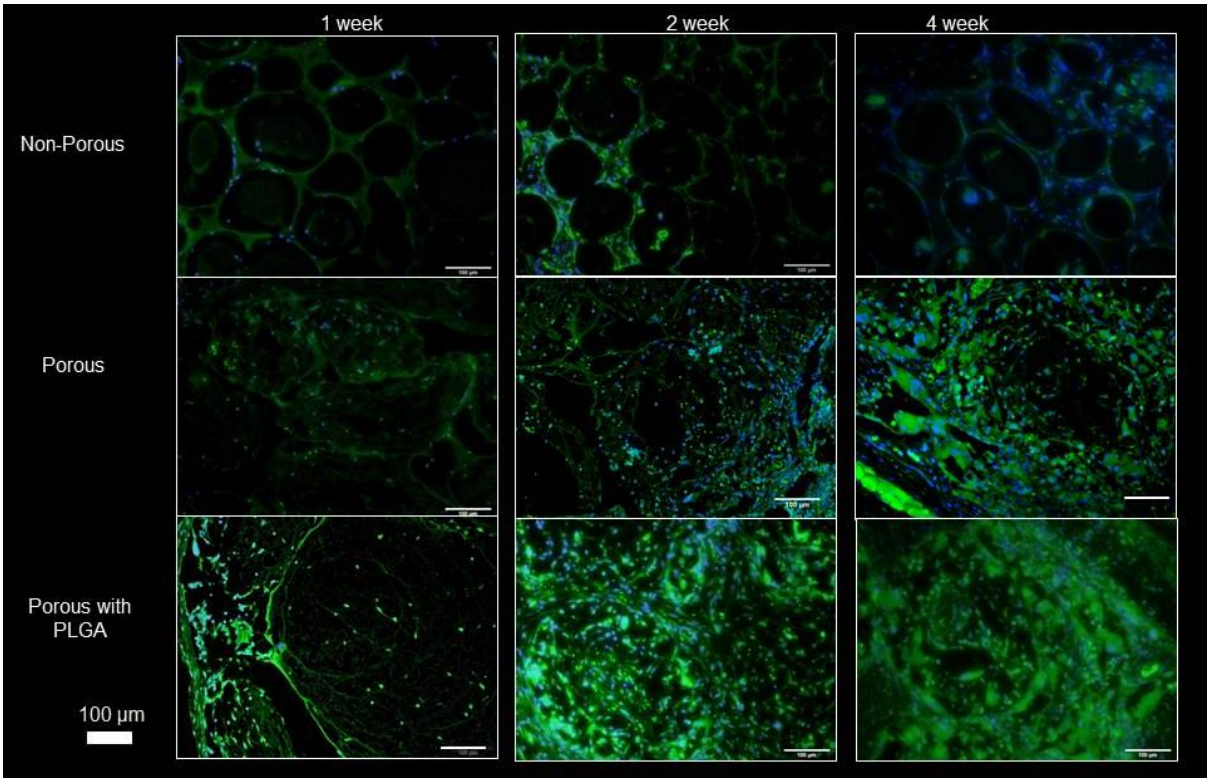

Figure 4-5. Immunohistochemistry of CD68 to identify monocytes and macrophages (green fluorescence). DAPI stained nuclei indicating nucleated cells (blue fluorescence). Scale bar = 100µm. Magnification 200X.

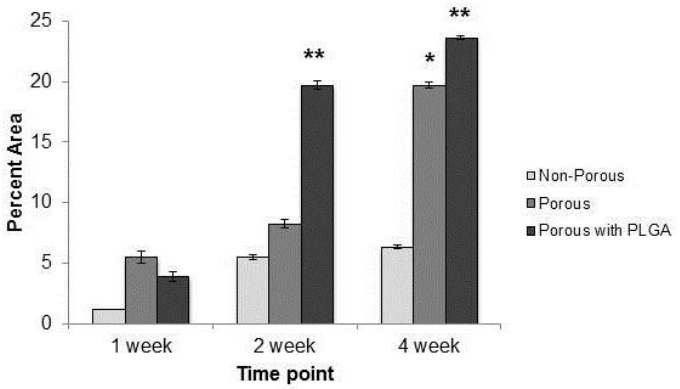

Figure 4-6. Quantification of CD68 staining. Statistical Analysis performed using student's t-test with $p<0.05$ indicating significance. * denotes statistical significance between porous and non-porous PCL particles. ** denotes statistical significance between PLGA coated and porous PCL particles.

4.4 Discussion

Macroporous microparticles offer many advantages *in vivo* compared to the non-porous traditional microspheres. Macroporous particles allow for cell infiltration into the interior portions of the particles whereas non-porous particles only have cells which maneuver around the whole particle. In order for non-porous particles to act as a tissue filler, they must have fibrous encapsulation and the formation of fibroplasias to keep them in place (14). The macroporous particles allow for the existing tissue cells to move in and therefore the PCL particles become an extension of the existing soft tissue network. Furthermore, the matrix deposition and healing response are accelerated with the addition of a PLGA coating onto the macroporous PCL microparticles.

Wound healing is part of the innate response within the body. First, hemostasis is achieved, followed by inflammation, proliferation, and remodeling (32). To determine the implant's ability to integrate into the tissue, extracellular matrix deposition and vascularization were analyzed to show that the proliferation phase had begun. The implants which contained macroporous particles had significantly greater collagen deposition and average blood vessel quantity and infiltration depth than the non-porous samples (Fig. 4-4) which elucidated incorporation of the particles with the body.

Tissue integration is important to hold the particles in place and allow the volume augmentation to be maintained. For this to occur, the wound healing process must allow fibroblasts to infiltrate the implant and begin producing extracellular matrix (32). In the explants (Figure 4-1), various cell types have infiltrated into the scaffolds by 4 weeks. Collagen production is a good determinant of extracellular matrix (ECM) deposition and tissue integration because collagen type I composes a majority of the ECM in the body. Skin is composed of about 80% collagen type I and 15% collagen type III (33). The picrosirius red staining data

suggests that the macroporous samples are beginning to have collagen deposited and to integrate them into existing tissue (Fig. 4-2).

To determine vascularization around the implanted material, immunohistochemical analysis with anti-CD31was used. CD31 is a specific marker for endothelial cells. CD31 can also be expressed on stem cells and monocytic cells, however it is prominent in endothelial cells. This can be seen in figure 4-3. Vascularization is important because it is noted that with a lower blood supply, soft tissue is more likely to recess (34), therefore it is suggested that with a stable vascular structure, tissue augmentation could be maintained. Red blood cells were often visible in the blood vessels within the implants, however they were not tested for functionality and connection to existing host vasculature.

Since it has been shown that implant survivability in other tissue models is enhanced due to complete tissue integration (28,35), the healing response can be accelerated to minimize migration and encourage integration. To encourage accelerated healing, poly(lactic-co-glycolic acid) (PLGA) was coated onto the macroporous PCL microparticles. PLGA is FDA approved and used in many different biomaterials due to it biodegradability (1); PLGA degrades by ester hydrolysis in the presence of water and its monomer units are recognized as by-products to metabolic pathways within the body (36). There are various formulations of PLGA; depending on the processing parameters of polymerization, the percentages of lactic acid and glycolic acid can vary. Acid modified PLGA has the same chemical make-up as the standard PLGA, only the end groups are carboxyl groups instead of being ester capped (as in hydrophobic PLGA). Acid modified PLGA has been shown to have faster degradation times (37,38). The time to degradation is important to allow for an acute response to the material, but then have the acid-modified PLGA degrade away. Additionally, PLGA has been shown to result in a faster healing rate (wound occlusion) *in vivo* with a porcine aneurysm model (31,39). It is suspected that the decrease in healing time is generated due to a local inflammatory response caused by the acid-

modified PLGA. PLGA has been shown to elicit an inflammatory response when cultured *in vitro* with dermal fibroblasts and monocytes (see results in Chapter 3), therefore it was expected that if we utilized the acid modified PLGA in a dermal model, the acute inflammatory response could be harnessed to result in matrix deposition more quickly because you would speed through the inflammatory phase of wound healing and more quickly initiate the proliferation and remodeling phases. PLGA, similar to that in the vascular aneurysm model, exhibited a similar response in the soft tissue implants presented here. CD68 was up-regulated in the macroporous PCL samples coated in PLGA as compared to the PCL alone at 2 weeks and 4 weeks (Fig. 4-6). Following the increase in inflammation, there was an increase in collagen deposition and blood vessel infiltration over the four week time course of the experiments (Fig. 4-2 and 4-3, respectively) which suggests that the tissue integrated even more quickly when the inflammatory response is stimulated.

A faster time course of inflammation to extracellular matrix deposition was reached by adding the PLGA coating onto the macroporous PCL particles. Although the pores alone allowed for greater cell infiltration, collagen deposition and vascularization over the non-porous particles (Fig. 4-4), the PLGA further stimulated the *in vivo* response to these particles by allowing for an even more robust reaction (Fig. 4-4 and 4-6). The increase in CD68 was expected due to the known inflammatory response of PLGA *in vitro* (see Chapter 3) and *in vivo* (40). Additionally, the collagen deposition that followed illustrates the translational ability of PLGA to stimulate the wound healing response in multiple tissue systems including a vascular response (31,39,41) and our soft tissue response.

This murine model has illustrated the potential of complete tissue integration of the novel macroporous PCL microparticles and how they have clinical potential for tissue augmentation. Additionally, this research has shown that the innate tissue response and normal wound healing can be harnessed to elicit an acute immune response and result in accelerated tissue

regeneration and subsequent healing due to the addition of bioactive PLGA. It is proposed that this combination of macroporous PCL microparticles with a bioactive PLGA coating can account for a short-lived immune response and long term stability which were weaknesses seen in existing injectable tissue augmentation materials.

4.5 References

1. Gunatillake PA, Adhikari R. Biodegradable synthetic polymers for tissue engineering. Eur Cell Mater. 2003 May 20;5:1–16; discussion 16.
2. Woodruff MA, Hutmacher DW. The return of a forgotten polymer—Polycaprolactone in the 21st century. Prog Polym Sci. 2010 Oct;35(10):1217–56.
3. Saralidze K, Koole LH, Knetsch MLW. Polymeric Microspheres for Medical Applications. Materials. 2010 Jun 7;3(6):3537–64.
4. Girones Molera J, Mendez JA, San Roman J. Bioresorbable and nonresorbable polymers for bone tissue engineering. Curr Pharm Des. 2012;18(18):2536–57.
5. Ravichandran R, Sundarrajan S, Venugopal JR, Mukherjee S, Ramakrishna S. Advances in polymeric systems for tissue engineering and biomedical applications. Macromol Biosci. 2012 Mar;12(3):286–311.
6. Chung EJ, Sugimoto M, Koh JL, Ameer GA. Low-pressure foaming: a novel method for the fabrication of porous scaffolds for tissue engineering. Tissue Eng Part C Methods. 2012 Feb;18(2):113–21.
7. Mikos AG, Temenoff JS. Formation of highly porous biodegradable scaffolds for tissue engineering. Electron J Biotechnol. 2000 Aug;3(2):23–4.
8. Mehdizadeh H, Sumo S, Bayrak ES, Brey EM, Cinar A. Three-dimensional modeling of angiogenesis in porous biomaterial scaffolds. Biomaterials. 2013 Apr;34(12):2875–87.
9. Ehsan SM, George SC. Nonsteady state oxygen transport in engineered tissue: implications for design. Tissue Eng Part A. 2013 Jun;19(11-12):1433–42.

10. Han L-H, Lai JH, Yu S, Yang F. Dynamic tissue engineering scaffolds with stimuli-responsive macroporosity formation. Biomaterials. 2013 Jun;34(17):4251–8.
11. Singh S, Wu BM, Dunn JCY. Accelerating Vascularization in Polycaprolactone Scaffolds by Endothelial Progenitor Cells. Tissue Eng Part A. 2011 Jul;17(13-14):1819–30.
12. Taboas J., Maddox R., Krebsbach P., Hollister S. Indirect solid free form fabrication of local and global porous, biomimetic and composite 3D polymer-ceramic scaffolds. Biomaterials. 2003 Jan;24(1):181–94.
13. Lightner DJ. Review of the available urethral bulking agents. Curr Opin Urol. 2002 Jul;12(4):333–8.
14. Jones DH. Semipermanent and permanent injectable fillers. Dermatol Clin. 2009 Oct;27(4):433–444, vi.
15. Greco TM, Antunes MB, Yellin SA. Injectable fillers for volume replacement in the aging face. Facial Plast Surg FPS. 2012 Feb;28(1):8–20.
16. Eppley BL, Dadvand B. Injectable soft-tissue fillers: clinical overview. Plast Reconstr Surg. 2006 Sep 15;118(4):98e–106e.
17. Funt D, Pavicic T. Dermal fillers in aesthetics: an overview of adverse events and treatment approaches. Clin Cosmet Investig Dermatol. 2013;6:295–316.
18. Lowe NJ, Maxwell CA, Patnaik R. Adverse reactions to dermal fillers: review. Dermatol Surg Off Publ Am Soc Dermatol Surg Al. 2005 Nov;31(11 Pt 2):1616–25.
19. Lemperle G, Romano JJ, Busso M. Soft Tissue Augmentation With Artecoll: 10-Year History,Indications, Techniques, and Complications. Dermatol Surg. 2003;29(6):573–87.
20. Bobyn JD, Jacobs JJ, Tanzer M, Urban RM, Aribindi R, Sumner DR, et al. The susceptibility of smooth implant surfaces to periimplant fibrosis and migration of polyethylene wear debris. Clin Orthop. 1995 Feb;(311):21–39.

21. Corrin AA, Ngai M, Walthers CM, Dunn JCY, Wu BM. Injectable macroporous microparticles for soft tissue augmentation. 2012 Annual International Conference of the IEEE Engineering in Medicine and Biology Society (EMBC). 2012. p. 2428 –2431.
22. Ng KW, Hutmacher DW, Schantz J-T, Ng CS, Too H-P, Lim TC, et al. Evaluation of Ultra-Thin Poly(ε-Caprolactone) Films for Tissue-Engineered Skin. Tissue Eng. 2001 Aug;7(4):441–55.
23. Ilya Petrou MD. Novel polycaprolactone dermal filler gains popularity in Europe [Internet]. Cosmetic Surgery Times. 2010 [cited 2014 Jan 30]. Available from: http://cosmeticsurgerytimes.modernmedicine.com/%5Bnode-source-domain-raw%5D/news/modernmedicine/modern-medicine-feature-articles/novel-polycaprolactone
24. Loh XJ, Colin Sng KB, Li J. Synthesis and water-swelling of thermo-responsive poly(ester urethane)s containing poly(ε-caprolactone), poly(ethylene glycol) and poly(propylene glycol). Biomaterials. 2008 Aug;29(22):3185–94.
25. Ciardelli G, Chiono V, Vozzi G, Pracella M, Ahluwalia A, Barbani N, et al. Blends of Poly-(ε-caprolactone) and Polysaccharides in Tissue Engineering Applications. Biomacromolecules. 2005 Jul 1;6(4):1961–76.
26. Sinha VR, Bansal K, Kaushik R, Kumria R, Trehan A. Poly-ϵ-caprolactone microspheres and nanospheres: an overview. Int J Pharm. 2004 Jun 18;278(1):1–23.
27. Williams JM, Adewunmi A, Schek RM, Flanagan CL, Krebsbach PH, Feinberg SE, et al. Bone tissue engineering using polycaprolactone scaffolds fabricated via selective laser sintering. Biomaterials. 2005 Aug;26(23):4817–27.
28. Romano JJ, Iliff NT, Manson PN. Use of Medpor porous polyethylene implants in 140 patients with facial fractures. J Craniofac Surg. 1993 Jul;4(3):142–7.

29. Nicolete R, Santos DF dos, Faccioli LH. The uptake of PLGA micro or nanoparticles by macrophages provokes distinct in vitro inflammatory response. Int Immunopharmacol. 2011 Oct;11(10):1557–63.
30. Iwasaki Y, Sawada S, Ishihara K, Khang G, Lee HB. Reduction of surface-induced inflammatory reaction on PLGA/MPC polymer blend. Biomaterials. 2002 Sep;23(18):3897–903.
31. Murayama Y, Tateshima S, Gonzalez NR, Vinuela F. Matrix and Bioabsorbable Polymeric Coils Accelerate Healing of Intracranial Aneurysms Long-Term Experimental Study. Stroke. 2003 Aug 1;34(8):2031–7.
32. Diegelmann RF, Evans MC. Wound healing: an overview of acute, fibrotic and delayed healing. Front Biosci J Virtual Libr. 2004 Jan 1;9:283–9.
33. Guiha R, Khodeiry SE, Mota L, Caffesse R. Histological Evaluation of Healing and Revascularization of the Subepithelial Connective Tissue Graft. J Periodontol. 2001 Apr;72(4):470–8.
34. Weber L, Kirsch E, Müller P, Krieg T. Collagen Type Distribution and Macromolecular Organization of Connective Tissue in Different Layers of Human Skin. J Invest Dermatol. 1984 Feb;82(2):156–60.
35. Niechajev I. Porous Polyethylene Implants for Nasal Reconstruction: Clinical and Histologic Studies. Aesthetic Plast Surg. 1999 Nov 1;23(6):395–402.
36. Anderson JM, Shive MS. Biodegradation and biocompatibility of PLA and PLGA microspheres. Adv Drug Deliv Rev. 2012 Dec;64, Supplement:72–82.
37. Wiggins JS, Hassan MK, Mauritz KA, Storey RF. Hydrolytic degradation of poly(d,l-lactide) as a function of end group: Carboxylic acid vs. hydroxyl. Polymer. 2006 Mar 8;47(6):1960–9.

38. Tracy MA, Ward KL, Firouzabadian L, Wang Y, Dong N, Qian R, et al. Factors affecting the degradation rate of poly(lactide-co-glycolide) microspheres in vivo and in vitro. Biomaterials. 1999 Jun;20(11):1057–62.
39. Murayama Y, Viñuela F, Tateshima S, Gonzalez NR, Song JK, Mahdavieh H, et al. Cellular Responses of Bioabsorbable Polymeric Material and Guglielmi Detachable Coil in Experimental Aneurysms. Stroke. 2002 Apr 1;33(4):1120–8.
40. Yoon SJ, Kim SH, Ha HJ, Ko YK, So JW, Kim MS, et al. Reduction of inflammatory reaction of poly(d,l-lactic-co-glycolic Acid) using demineralized bone particles. Tissue Eng Part A. 2008 Apr;14(4):539–47.
41. Yuki I, Uchiyama N, Murayama Y, Nien Y-L, Lee D, Ebara M, et al. Intravascular tissue reactions induced by various types of bioabsorbable polymeric materials: correlation between the degradation profiles and corresponding tissue reactions. Neuroradiology. 2010 Nov;52(11):1017–24.

CHAPTER FIVE

CONCLUSIONS AND FUTURE DIRECTIONS

5.1 List of Novel Findings

Particles

- Wide range of microparticle sizes are achieved while maintaining macroporosity
- PCL macroporous particles are spray coated with an additional polymeric material (PLGA)

In vitro

- 3D human cell co-culture to measure inflammatory response to biomaterials
- Increase in IL-1β, IL-6, GM-CSF, and TNF-α expression from a human cell co-culture due to the addition of PLGA

In vivo

- PCL Macroporous microparticles allow for blood vessel infiltration throughout the pores
- PLGA coating on PCL macroporous microparticles initiates an inflammatory response and results in collagen deposition throughout the particles
- Accelerated healing around the PLGA coated microparticles when compared to the macroporous PCL particles alone

5.2 Clinical Applications of Novel Biomaterial

Preliminary trials have been performed to show proof of concept for using the macroporous PCL microparticles for applications in tissue augmentation. The three *in vivo* applications are: dermal filler, periurethral bulking and gingival augmentation (Fig. 5-1). The macroporous microparticles show promise as a way to augment soft tissue and with the bioactive PLGA coating, can accelerate healing times. The bioactive PLGA coating has exhibited the ability to activate an immune response (see Chapter 3 and 4) and also decrease

healing times (see Chapter 4). The result is more significant extracellular matrix production in a lessened amount of time.

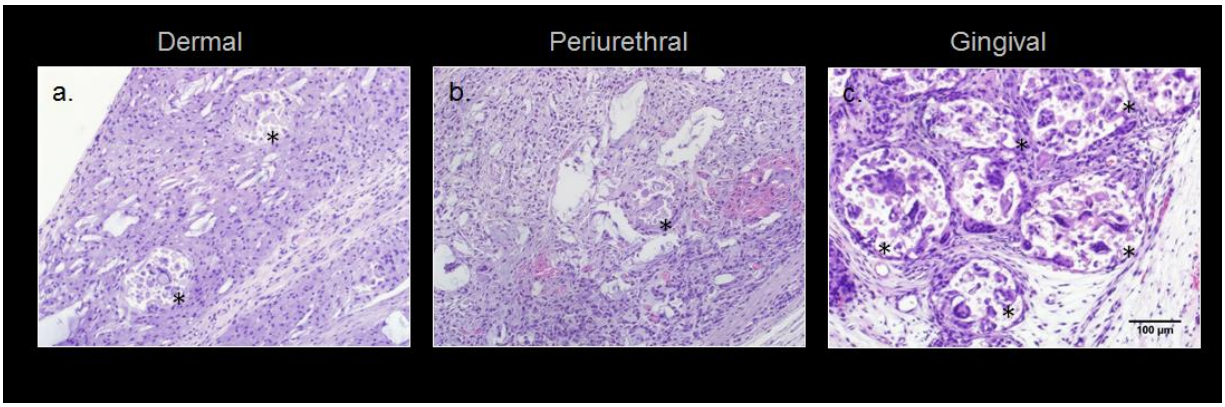

Figure 5-1 Injected macroporous PCL microparticles. **a.** Subcutaneous dermal injection harvested at 8 weeks **b.** Periurethal injection adjacent to the bladder harvested at 3 weeks **c.** Gingival injection harvested at 2 weeks. ***** Denotes particles in the injection site. Scale bar = 100 µm.

As seen in Fig. 5-2 the macroporous particles injected subcutaneously in a rat model, have a significant amount of cell in-growth and extracellular matrix deposition after 8 weeks. The PLGA coating appears to qualitatively increase the amount of collagen deposition in and around the particles as seen in Fig. 5-2.

For preliminary experimental design on urethral bulking, particles were injected periurethrally and subsequently the urethra and bladder were harvested at various time points. The images show the particles in the periurethral area (Fig. 5-3) and there are ongoing urinary flow experiments to show functionality using the new bulking agent. Qualitatively, the particles have good tissue integration and collagen deposition in and around the injection site either adjacent to the bladder (Fig. 5-3a), at the bladder neck (Fig. 5-3b), or in the urethra (Fig. 5-3c).

The gingival augmentation was performed in the tight and mucosal regions of the rat gingiva. The particles were injected, then the area was harvested two weeks later for analysis. From the H&E stained images, you see cell infiltration and inflammation throughout the particles and the area of injection (Fig. 5-1c.). Additionally, there is collagen deposition around the particles in the macroporous PCL injection (Fig. 5-4a,c), whereas there is some collagen growing throughout the particles in the PLGA coated samples (Fig. 5-4b,d).

Together the dermal and gingival augmentation preliminary studies suggest that with the PLGA coating, you achieve collagen deposition throughout the particles, whereas with PCL alone in the small particle size range, there is only deposition of collagen around the particles. The periurethral data is very preliminary and more studies must be done to show the efficacy and results from the periurethral injections.

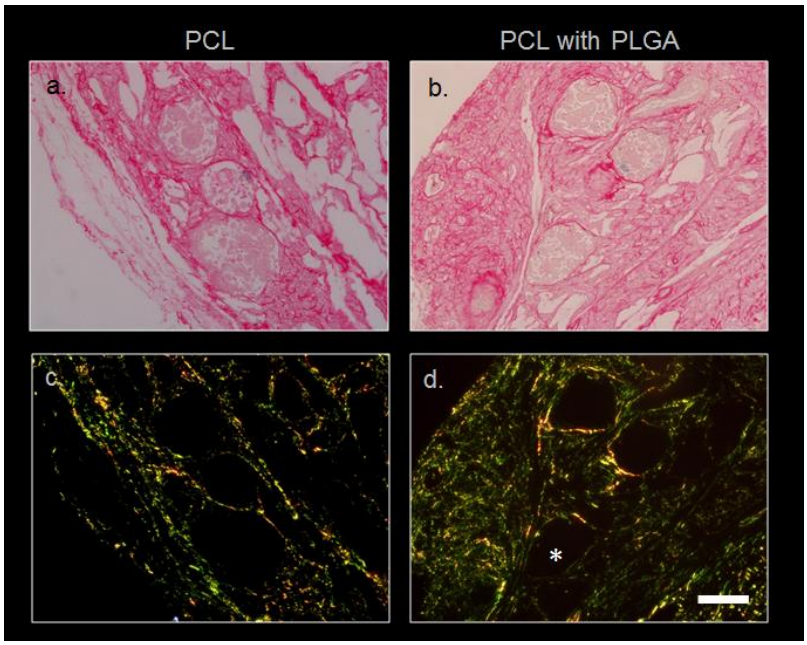

Figure 5-2 Collagen deposition with picrosirus red staining in rat subcutaneous dermal injection. **a, c**. macroporous PCL microparticles harvested at 8 weeks **b,d.** macroporous PCL microparticles with PLGA coating harvested at 8 weeks **c,d.** polarized light images showing the birefringence of the developed collagen fibers. ***** denotes collagen deposited inside the particle. Scale bar = 100 µm.

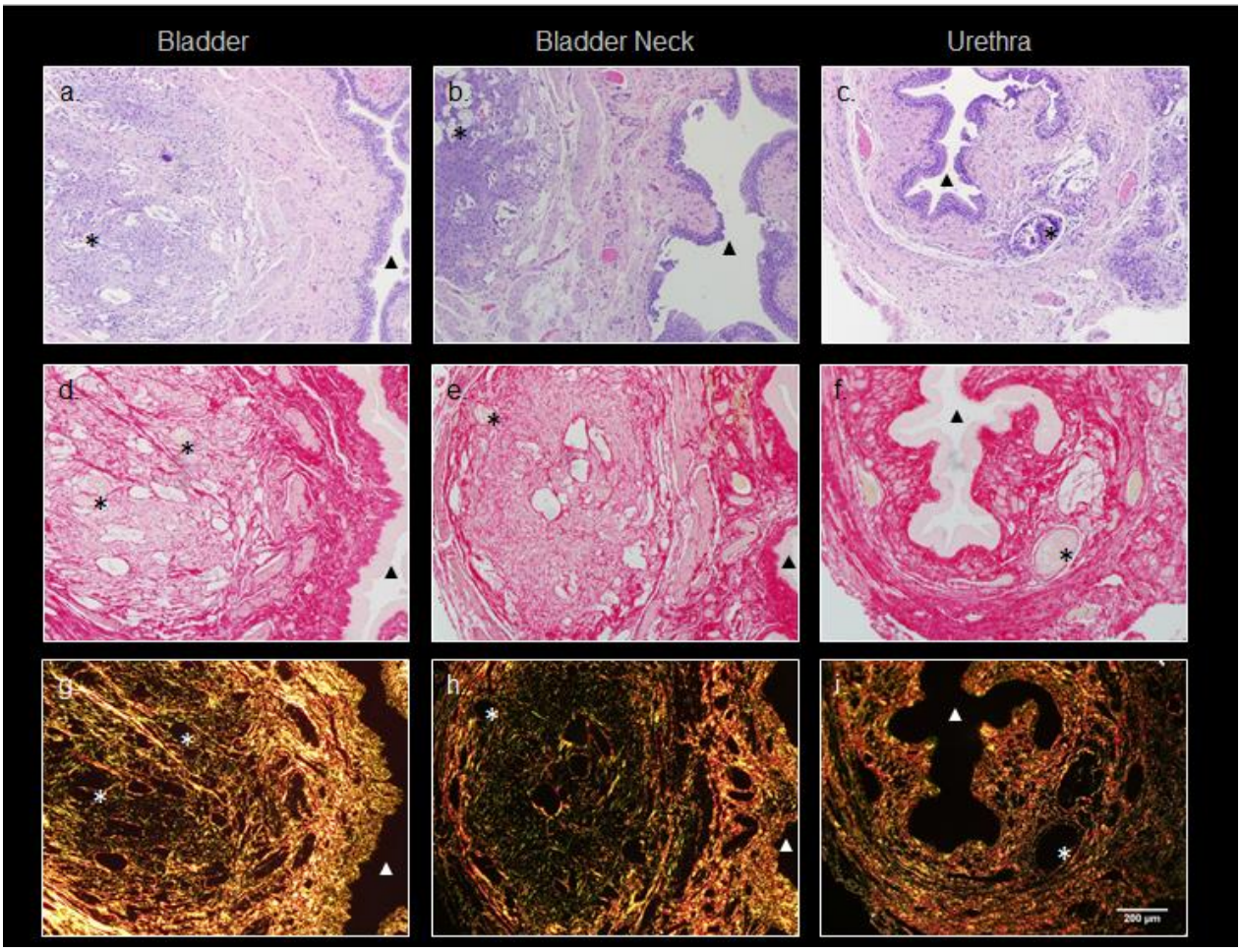

Figure 5-3 Periurethral Injections of macroporous PCL microparticles harvested at 12 weeks **a, d, g** Injections near bladder. **b, e, h** Injections near bladder neck. **c, f, j** Injections near urethra. **a-c**. H&E images of paraffin embedded samples. **d-f.** Picrosirius Red images in brightfield. **g-i.** Picrosirius Red staining under polarized light showing the birefringence of the developed collagen fibers. Scale bar = 200 µm. ▲ denotes intraluminal space. ***** denotes particles within injection site.

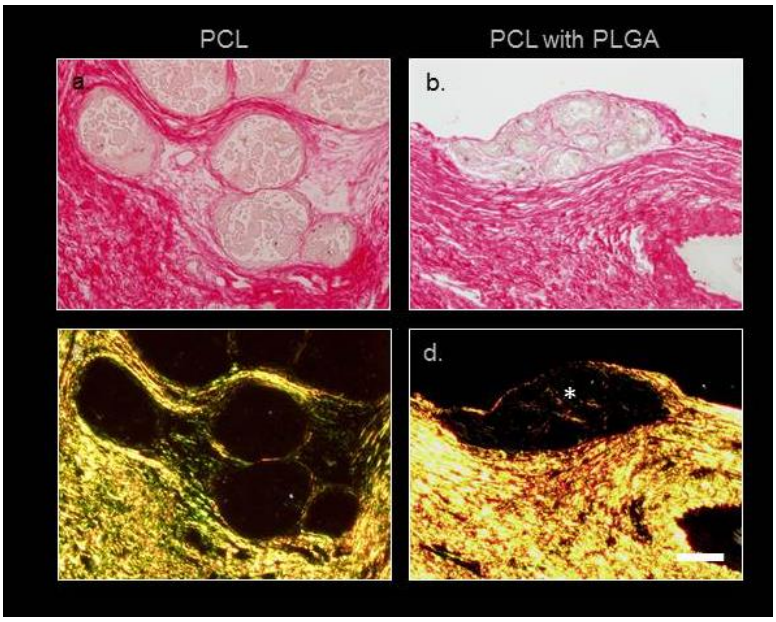

Figure 5-4 Collagen deposition with picrosirus red staining in rat gingival injection. **a, c**. macroporous PCL microparticles harvested at 2 weeks **b,d.** macroporous PCL microparticles with PLGA coating harvested at 2 weeks **c,d.** polarized light images showing the birefringence of the developed collagen fibers. ***** denotes collagen deposited inside the particle. Scale bar = 100 µm.

5.3 Conclusions and Future Directions of Research

The research has demonstrated potential for clinical use of a novel biomaterial. The fabrication techniques for the macroporous PCL microparticles should be easily scalable for large applications and commercial marketing. The significance of the novel biomaterial is the macroporosity, injectability, ease of use, lifetime *in vivo* and variable application potential. The macroporosity allows cells to infiltrate into the particles and integrate the particles into the existing soft tissue matrix. This has been demonstrated with multiple *in vivo* pilot studies (see Chapter 4 and Figure 5-1). The injectability leads to a less significant procedure as compared to a surgical incision, implantation and suturing method. This can potentially benefit a patient by decreasing recovery and healing times. The ease of use of the macroporous particles which are easily suspended in an injection medium allows personnel to feel comfortable with the use of the material. The lifetime *in vivo* of PCL is known to be on the order of years, yet it is still a biodegradable material. The advantages of this is the structural stability of the material for the first few years as the native tissue is growing in an around the implant and maturing. Then the material will degrade away, however this is on a slow enough time scale that the tissue augmentation has already occurred. The size range of the macroporous PCL microparticles make them ideal for many augmentation applications of soft tissue.

The addition of the bioactive PLGA coating allows for a transient immune response resulting in accelerated healing times around the macroporous microparticles. The specific cytokines involved in inflammation of the bioactive PLGA coating have been investigated *in vitro* (see Chapter 3). The understanding of the interaction of a cellular co-culture and the reaction of the co-culture to a biomaterial is very important and was achieved through the 3D model developed in this research. This *in vitro* model corroborates to the *in vivo* data showing significantly increased inflammation earlier on as compared to the macroporous PCL microparticles alone. The increase in inflammation (IL-1β, IL-6, GM-CSF, and TNF-α) is

therefore believed to contribute to the decrease in healing times shown *in vivo*. Healing time is assessed to decrease based on increased collagen deposition and an increase in the number of blood vessels (see Chapter 4). These two investigations contribute to the particles being integrated into the tissue by extracellular matrix deposition and vascular connection indicating healing.

For continued progress on bringing the macroporous microparticles to clinical market, more *in vivo* testing must be performed to investigate long term stability of the material. A clear direction of product use must be established in order to obtain estimated market and investment worth. After more thorough animal studies have been performed, recommended particle size and dosage can be determined for clinical application. Subsequently, a 510(k) process for material approval will be needed before clinical trials begin. Due to the fact that the polymeric materials included in the biomaterials are previously used in FDA approved devices, this should aid in the approval process and ease of use of this material in the commercial industry.